IRF4 controls the positioning of mature B cells in the lymphoid microenvironments by regulating NOTCH2 expression and activity

Giorgia Simonetti,[1] Amanda Carette,[1] Kathryn Silva,[1] Haowei Wang,[4] Nilushi S. De Silva,[1] Nicole Heise,[1] Christian W. Siebel,[7] Mark J. Shlomchik,[4,5,6] and Ulf Klein[1,2,3]

[1]Herbert Irving Comprehensive Cancer Center, [2]Department of Pathology and Cell Biology, and [3]Department of Microbiology and Immunology, Columbia University, New York, NY 10032
[4]Department of Laboratory Medicine and [5]Department of Immunobiology, Yale University School of Medicine, New Haven, CT 06520
[6]Department of Immunology, University of Pittsburgh School of Medicine, Pittsburgh, PA 15261
[7]Department of Molecular Biology, Genentech, Inc., South San Francisco, CA 94080

The transcription factor interferon regulatory factor-4 (IRF4) is expressed in B cells at most developmental stages. In antigen-activated B cells, IRF4 controls germinal center formation, class-switch recombination, and the generation of plasma cells. Here we describe a novel function for IRF4 in the homeostasis of mature B cells. Inducible deletion of *irf4* specifically in B cells in vivo led to the aberrant accumulation of *irf4*-deleted follicular B cells in the marginal zone (MZ) area. IRF4-deficient B cells showed elevated protein expression and activation of NOTCH2, a transmembrane receptor and transcriptional regulator known to be required for MZ B cell development. Administration of a NOTCH2-inhibitory antibody abolished nuclear translocation of NOTCH2 in B cells within 12 h and caused a rapid and progressive disintegration of the MZ that was virtually complete 48 h after injection. The disappearance of the MZ was accompanied by a transient increase of MZ-like B cells in the blood rather than increased B cell apoptosis, demonstrating that continued NOTCH2 activation is critical for the retention of B cells in the MZ. Our results suggest that IRF4 controls the positioning of mature B cells in the lymphoid microenvironments by regulating NOTCH2 expression. These findings may have implications for the understanding of B cell malignancies with dysregulated IRF4 and NOTCH2 activity.

CORRESPONDENCE
Ulf Klein:
uk30@columbia.edu

Abbreviations used: CLL, chronic lymphocytic leukemia; FO, follicular; GC, germinal center; GEP, gene expression profiling; IC, intracellular; IF, immunofluorescence; IHC, immunohistochemistry; MZ, marginal zone; qRT-PCR, quantitative RT-PCR; SMZL, splenic MZ lymphoma; TAM, tamoxifen.

IRF4 is a member of the interferon regulatory factor (IRF) family of transcription factors and exerts critical functions in various cell types of the immune system (De Silva et al., 2012). In the B cell lineage, IRF4 is expressed in all developmental stages, with the exception of germinal center (GC) B cells (Falini et al., 2000; Cattoretti et al., 2006). During the generation of B cells in the bone marrow, IRF4 is largely redundant with the IRF family member IRF8 (Lu et al., 2003). The study of *irf4* knockout mice revealed that IRF4 is required for T cell–dependent antibody responses (Mittrücker et al., 1997), and subsequent work demonstrated that IRF4 is critically involved in the initiation and termination of the GC reaction, immunoglobulin class-switch recombination, and plasma cell differentiation (Klein et al., 2006; Sciammas et al., 2006; Saito et al., 2007; Ochiai et al., 2013). There is emerging evidence that during these mechanistically distinct processes, IRF4 exerts its different functions through interaction with stage-specific cofactors and through a graded expression (Sciammas et al., 2006, 2011; Ochiai et al., 2013) that reaches its highest levels in plasma cells.

Reflecting the diverse, context-dependent functions of IRF4 in different B lineage subsets, deregulation of the biological programs controlled by IRF4 has been linked to the pathogenesis of several types of B cell tumors corresponding to various developmental stages (Shaffer et al.,

The Rockefeller University Press $30.00
J. Exp. Med. 2013 Vol. 210 No. 13 2887-2902
www.jem.org/cgi/doi/10.1084/jem.20131026

The Journal of Experimental Medicine

2009, 2012; De Silva et al., 2012). As such, IRF4 is unusual in comparison with other lymphoma-related transcriptional regulators in that it is associated with oncogenic as well as tumor-suppressor functions. IRF4 has oncogenic roles in several GC and post-GC B cell malignancies, including multiple myeloma, subtypes of diffuse large B cell lymphoma, and Hodgkin lymphoma. Conversely, IRF4 exerts potential tumor-suppressor functions in B cell acute lymphoblastic leukemia, a malignancy deriving from immature B cells, and in chronic lymphocytic leukemia (CLL), a tumor of quiescent mature B cells.

The first evidence that IRF4 may have a unique role in the regulation of the peripheral B cell compartment stemmed from the observation that *irf4* knockout mice, despite normal surface expression of IgM and of κ and λ light chains, displayed a different B cell immunophenotype compared with wild-type mice (Mittrücker et al., 1997). In particular, IRF4-deficient B cells expressed lower amounts of CD23, a finding which led Mittrücker et al. (1997) to propose that these cells are blocked at a late, transitional stage of peripheral B cell maturation. Subsequent studies suggested that IRF4-deficient B cells acquire a marginal zone (MZ) B cell–like immunophenotype, as the $CD23^-$ cells express high levels of the CD21 (Klein et al., 2006) and CD1d antigens (Ochiai et al., 2013) that are characteristic for splenic MZ B cells (Pillai and Cariappa, 2009).

MZ B cells localize at the border of the splenic white pulp (Pillai et al., 2005) and respond rapidly to blood-borne pathogens (Martin and Kearney, 2000). These cells are functionally, immunophenotypically, and histologically distinct from follicular (FO) B cells, which are primarily involved in T cell–dependent B cell responses. Studies with conditional knockout mouse models have revealed that the development of MZ versus FO B cells requires activation of the NOTCH pathway (Tanigaki et al., 2002) through the NOTCH2 receptor (Saito et al., 2003). Mice lacking expression of NOTCH2, the NOTCH ligand delta-like 1 (DLL1), or NOTCH signaling components show a dramatic decrease in the number of MZ B cells (Tanigaki et al., 2002; Saito et al., 2003; Hozumi et al., 2004; Tan et al., 2009). On the contrary, constitutive expression of the active form of NOTCH2 in B cells leads to a marked increase in the number of MZ versus FO B cells (Hampel et al., 2011). Although both IRF4 and NOTCH affect MZ versus FO B cell development, it is unclear whether and how these pathways are connected.

Using a conditional *irf4* allele and an inducible Cre-recombinase that is expressed specifically in B cells, we here show that inducible deletion of *irf4* in B cells leads to an accumulation of IRF4-deficient B cells in the MZ, which was associated with elevated protein expression and activation of NOTCH2. Inhibition of NOTCH2 activation reversed the observed phenotype, revealing that continued signaling through NOTCH2 is required for the retention of B cells in the MZ as well as, potentially, for the maintenance of MZ B cells. The results suggest that in quiescent mature B cells, IRF4 establishes a biological program that prevents B cell retention in the MZ through regulating NOTCH2 expression.

RESULTS

Abnormal tissue distribution of mature B cells in *irf4* knockout mice

$irf4^{-/-}$ mice are known to develop B cell expansions with an MZ phenotype ($CD19^+CD23^-CD21^{hi}CD1d^{hi}IgM^{hi}IgD^{lo}$) and concomitant loss of FO-type B cells ($CD19^+CD23^+CD21^{int}$-$CD1d^{lo}IgM^{lo/+}IgD^{hi}$) in the spleen (Mittrücker et al., 1997; Klein et al., 2006; Ochiai et al., 2013). However, the localization of $irf4^{-/-}$ B cells within the splenic microenvironments has not been studied. We therefore stained spleen sections of $irf4^{-/-}$, $irf4^{+/-}$, and $irf4^{+/+}$ mice with the MOMA1 antibody, which recognizes metallophilic macrophages located at the border between the FO and MZ areas. Whereas in wild-type and $irf4^{+/-}$ mice the majority of B cells localized in the FO area, B cells in $irf4^{-/-}$ mice preferentially localized in the MZ area (Fig. 1 A). Thus, mature B cells developing in *irf4* knockout mice show an abnormal distribution within the splenic microenvironments that is skewed toward an MZ localization.

Inducible deletion of *irf4* in mature B cells leads to their accumulation in the MZ

In $irf4^{-/-}$ mice, the deficiency of *irf4* in a variety of immune cell types and in B cells throughout development hampers analysis of the autonomous function of IRF4 in mature B cells. To assess the intrinsic role of IRF4 in quiescent mature B cells, we established a system that enables the inducible deletion of *irf4* specifically in B cells by crossing a conditional *irf4* allele (Klein et al., 2006) to mice that express a tamoxifen (TAM)-inducible Cre-recombinase from the human CD20 promoter (CD20-TAM-Cre; Fig. 1 B; Khalil et al., 2012). Through this approach, inducible deletion of *irf4* is associated with concomitant activation of eGFP expression, allowing the tracking of IRF4-deficient B cells (Klein et al., 2006). Deletion occurred in ∼25% of splenic lymphocytes, corresponding to ∼50% of B cells, upon TAM administration (Fig. 1, C and D). Loss of IRF4 protein expression upon Cre-mediated deletion was confirmed in $eGFP^+$ B cells flow sorted from the spleen of $irf4^{fl/fl}$CD20-TAM-Cre mice, whereas it was retained in $eGFP^+$ B cells purified from $irf4^{fl/+}$CD20-TAM-Cre mice (Fig. 1 E). The results demonstrate that eGFP expression constitutes a direct readout for biallelic ($irf4^{fl/fl}$) and monoallelic ($irf4^{fl/+}$) *irf4* gene deletion in B cells from *irf4*-conditional mice and allowed us to track deleted cells in the lymphoid tissues by flow cytometry (Fig. 1 D).

$irf4^{fl/fl}$CD20-TAM-Cre, $irf4^{fl/+}$CD20-TAM-Cre, and CD20-TAM-Cre mice were injected with TAM and analyzed for splenic B cell subpopulations at days 11–14 after the final injection. Flow cytometric analysis revealed no differences in the FO and MZ fractions of splenic B lymphocytes and in the percentage of *irf4*-deleted cells among the genotypes (Fig. 2 A and Table 1). In marked contrast, however, histological examination of spleen sections derived from $irf4^{fl/fl}$CD20-TAM-Cre, $irf4^{fl/+}$CD20-TAM-Cre, and CD20-TAM-Cre mice revealed the presence of significantly enlarged MZ areas in mice with homozygous deletion of *irf4* in B cells relative to controls (Fig. 2 B, left, H&E).

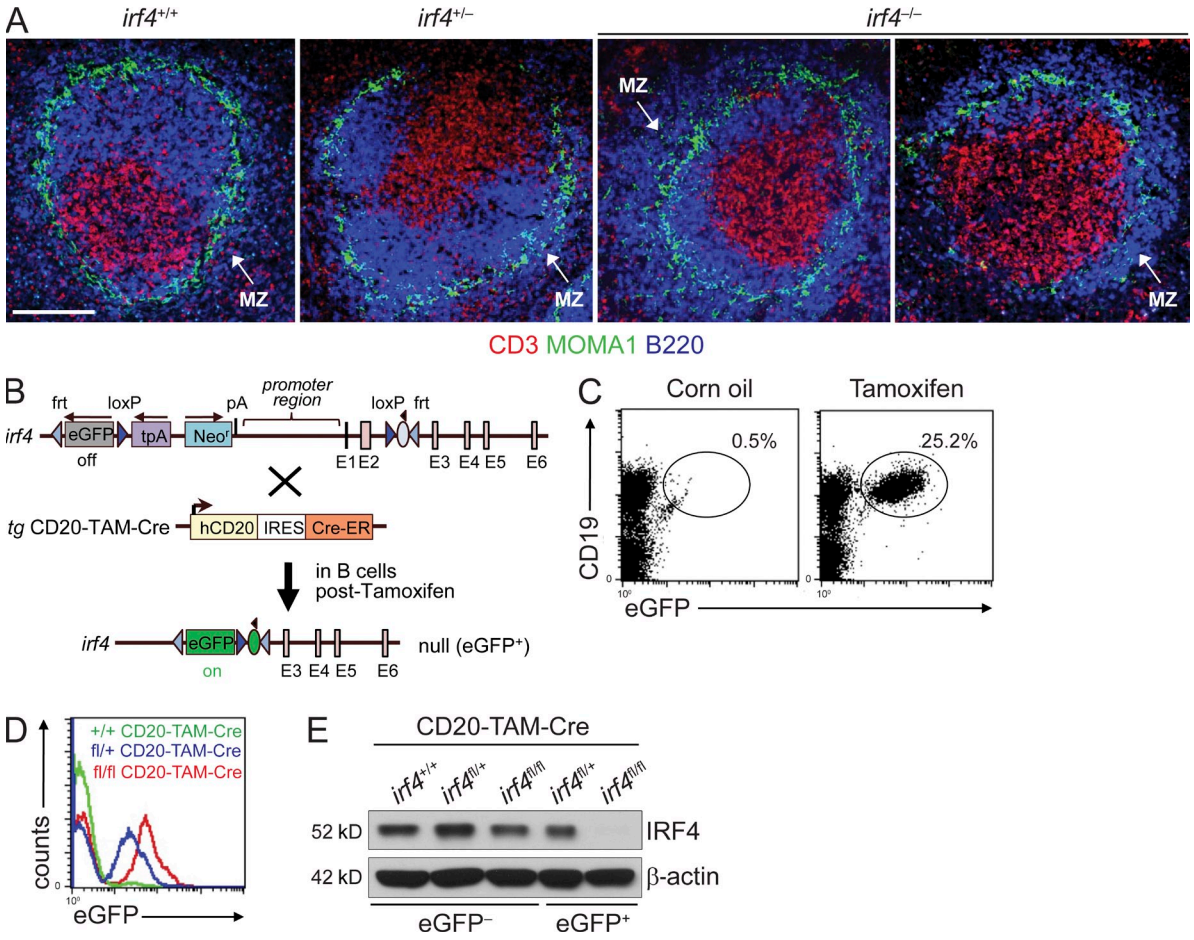

Figure 1. Preferential localization of B lymphocytes in the splenic MZ of *irf4*$^{-/-}$ mice and inducible deletion of *irf4* in B cells in vivo. (A) Spleen sections from *irf4*$^{+/+}$, *irf4*$^{+/-}$, and *irf4*$^{-/-}$ mice were analyzed for CD3, MOMA1, and B220 expression by IF. One representative mouse out of four per group is shown. Bar, 500 µm. (B) Schematic representation of the Cre-ER transgene under the control of the human (h) CD20 promoter (middle) and of the *irf4* gene before (top) and after (bottom) Cre-mediated recombination in the *irf4*$^{fl/fl}$CD20-TAM-Cre model. (C–E) Mice were challenged with three doses of TAM on three consecutive days and analyzed 11–14 d after the final TAM injection. (C) Spleen cells from *irf4*$^{fl/fl}$CD20-TAM-Cre mice after administration of corn oil or TAM (n = 4 per group, two independent experiments) were analyzed for CD19 and eGFP expression by flow cytometry. The number above the gate indicates percentage of eGFP+ B cells among lymphocytes. (D) eGFP expression level on splenic B cells from *irf4*$^{fl/fl}$CD20-TAM-Cre, *irf4*$^{fl/+}$CD20-TAM-Cre, and CD20-TAM-Cre mice was assessed by flow cytometry (one representative mouse out of four to eight per group is shown; four independent experiments). (E) B cells were sorted from the spleen of *irf4*$^{fl/fl}$CD20-TAM-Cre, *irf4*$^{fl/+}$CD20-TAM-Cre, and CD20-TAM-Cre mice, and IRF4 expression was determined by Western blot (one representative of two independent experiments).

We then used immunohistochemistry (IHC) analysis for eGFP in combination with IgM to track the localization of homozygous and heterozygous *irf4*-deleted B cells within the splenic microenvironments of *irf4*$^{fl/fl}$CD20-TAM-Cre and *irf4*$^{fl/+}$CD20-TAM-Cre mice. The results showed that homozygous deletion of *irf4* in B cells led to a significantly increased localization of eGFP^{+}IgM^{+} B cells in the MZ area (Fig. 2 B). Overall, we observed an ∼2.4-fold increase in the ratio of the MZ/lymphoid follicle areas in the *irf4*$^{fl/fl}$CD20-TAM-Cre mice compared with *irf4*$^{fl/+}$CD20-TAM-Cre and CD20-TAM-Cre mice (Fig. 2 C). The following observations indicate that the accumulation of eGFP^{+} B cells in the MZ of *irf4*$^{fl/fl}$CD20-TAM-Cre mice results from an increased B cell retention of IRF4-deficient FO B cells in the MZ area. First, whereas in *irf4*$^{fl/+}$CD20-TAM-Cre and CD20-TAM-Cre mice the MZ appeared as the characteristic sharp rim of cells expressing high levels of IgM at the outer boundary of the splenic white pulp, the MZ of *irf4*$^{fl/fl}$CD20-TAM-Cre mice was comprised of B cells expressing lower and variable levels of IgM (Fig. 2 D), as characteristically observed on FO B cells. In accordance with this observation, we detected an increased amount of IgD^{hi} B cells (which were mostly IgM$^{lo/+}$) in the MZ of *irf4*$^{fl/fl}$CD20-TAM-Cre mice compared with control mice (Fig. 2 E). Second, IHC staining for the proliferation marker Ki-67 revealed that the MZ enlargement in the *irf4*$^{fl/fl}$CD20-TAM-Cre mice was not associated with in situ B cell proliferation in the spleen (not depicted) and hence is not the result of an expansion of abnormally proliferating MZ B cells. Collectively, these results suggest that homozygous deletion of *irf4* in FO B cells alters their migratory properties.

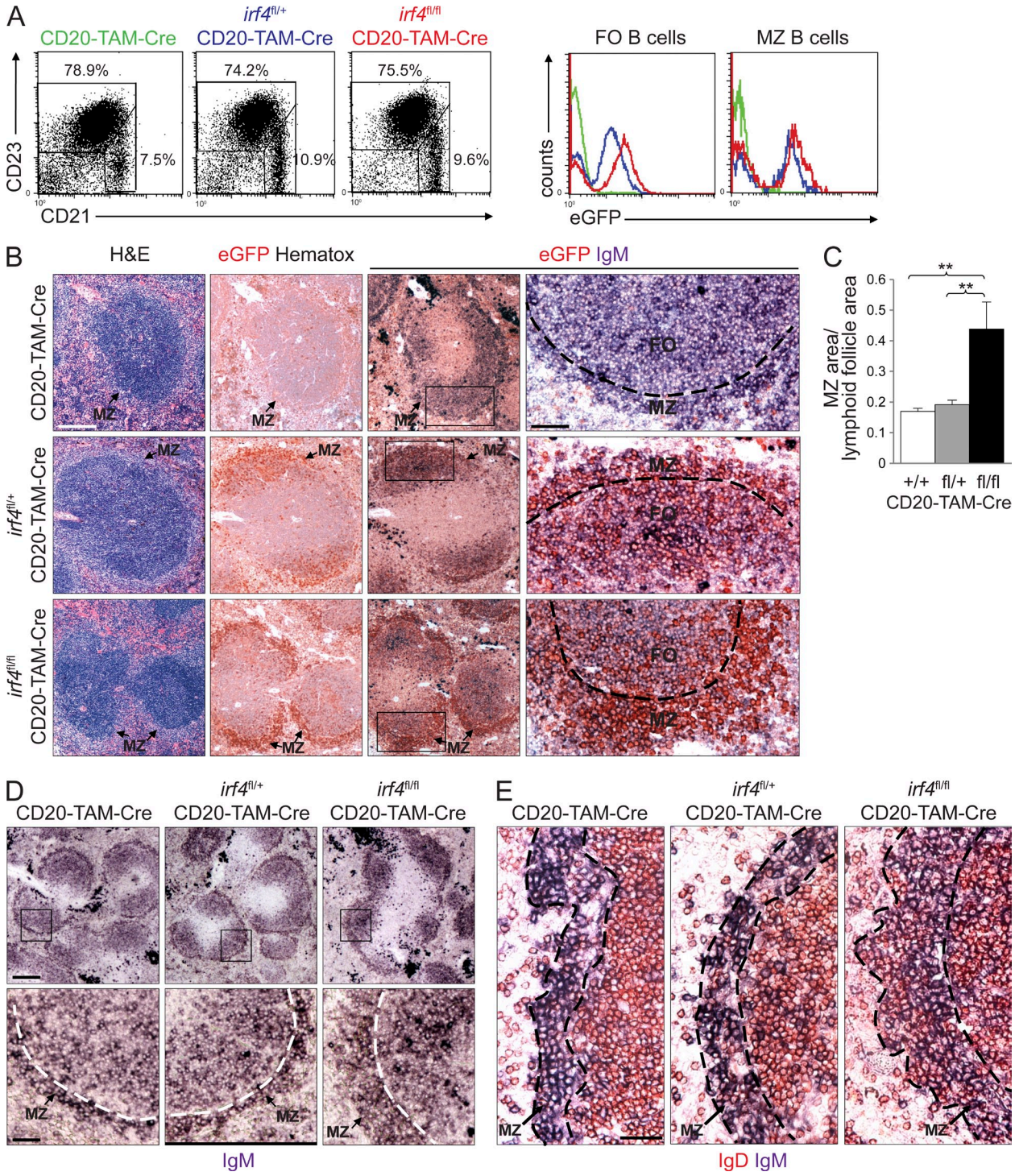

Figure 2. Preferential localization of B cells in the splenic MZ upon inducible B cell–specific deletion of *irf4*. *irf4*$^{fl/fl}$CD20-TAM-Cre, *irf4*$^{fl/+}$CD20-TAM-Cre, and CD20-TAM-Cre mice were injected with three doses of TAM on three consecutive days and analyzed 11–14 d after the last injection. Images show one representative mouse per group (*irf4*$^{fl/fl}$CD20-TAM-Cre: $n = 6$; *irf4*$^{fl/+}$CD20-TAM-Cre: $n = 8$; CD20-TAM-Cre: $n = 4$; four independent experiments), except for C. (A) CD21 and CD23 expression by CD19$^+$ splenic B cells from CD20-TAM-Cre, *irf4*$^{fl/+}$CD20-TAM-Cre, and *irf4*$^{fl/fl}$CD20-TAM-Cre mice were analyzed by flow cytometry. Numbers above gates indicate the percentage of CD23$^+$CD21^{int} FO and CD23$^-$CD21^{hi} MZ B cells. (right) eGFP expression by splenic FO and MZ B cells from CD20-TAM-Cre (green lines), *irf4*$^{fl/+}$CD20-TAM-Cre (blue lines), and *irf4*$^{fl/fl}$CD20-TAM-Cre (red lines) mice was assessed by flow cytometry. (B) Spleen sections from CD20-TAM-Cre, *irf4*$^{fl/+}$CD20-TAM-Cre, and *irf4*$^{fl/fl}$CD20-TAM-Cre mice were stained with H&E or analyzed for expression of eGFP counterstained with hematoxylin or with anti-IgM. Boxes demarcate the area shown at higher magnification to the right. (C) Ratio between the MZ and the lymphoid follicle areas in the spleen of CD20-TAM-Cre (+/+), *irf4*$^{fl/+}$CD20-TAM-Cre (fl/+), and *irf4*$^{fl/fl}$CD20-TAM-Cre (fl/fl) mice

Table 1. Frequencies of CD19+, MZ, FO, and eGFP+ B cells in the spleen of *irf4*^{floxed}CD20-TAM-Cre mice at days 11–14 after TAM administration

Genotype	% CD19+ cells	Among CD19+ cells		% eGFP+CD19+ cells	% eGFP+ B cells	
		% MZ	% FO		Among MZ	Among FO
irf4$^{+/+}$CD20-TAM-Cre (n = 4)	45.6 ± 5.2	8.5 ± 1.2	79.8 ± 3.0	1.7 ± 0.5	-	-
irf4$^{fl/+}$CD20-TAM-Cre (n = 8)	39.3 ± 7.2	10.2 ± 1.6	75.4 ± 4.2	49.9 ± 6.6	56.5 ± 8.0	55.6 ± 4.1
irf4$^{fl/fl}$CD20-TAM-Cre (n = 6)	42.1 ± 5.5	8.4 ± 1.2	74.9 ± 2.6	54.1 ± 12.4	60.5 ± 10.2	58.2 ± 10.1

irf4–deleted B cells show differential expression of genes with functions in trafficking

To identify genes contributing to the altered migratory properties of IRF4-deficient B cells, we performed gene expression profiling (GEP) analysis of B cells from the spleens of *irf4*$^{-/-}$ and *irf4*$^{+/+}$ mice. Having established B cell autonomy of the observed migratory phenotype (Fig. 2), we performed molecular analysis on IRF4-deficient B cells using constitutional *irf4*-deleted mice, as this allowed us to purify large numbers of B cells by magnetic cell separation, which is less harsh for the cells than flow sorting. Supervised analysis identified changes in the expression of 86 genes (68 up- and 18 down-regulated) in *irf4*$^{-/-}$ versus *irf4*$^{+/+}$ B cells, which were organized into putative functional categories (Fig. 3 A). Compared with a published GEP analysis of MZ versus FO B lymphocytes (Kin et al., 2008), 11 of the 86 differentially expressed genes showed the same trend of expression in *irf4*$^{-/-}$ versus *irf4*$^{+/+}$ B cells (underlined in Fig. 3 A), indicating that the IRF4 signature in quiescent mature B cells comprises a subset of genes that is differentially expressed in MZ and FO B cells.

A particularly relevant finding with regard to the observed migratory phenotype was the enrichment in genes with known functions in cell migration and homing that were altered in expression in B cells from IRF4-deficient mice. mRNAs encoding two such genes were down-regulated in IRF4-deficient compared with wild-type B cells, namely regulator of G-protein signaling 13 (RGS13), which dampens the B cell response to chemokines (Shi et al., 2002), and the activated leukocyte cell adhesion molecule (ALCAM/CD166), which controls migration processes in various cell types (Cayrol et al., 2008) and which is down-regulated in MZ versus FO B cells (Kin et al., 2008). Conversely, mRNAs encoding Plexin-D1 (PLXND1), a semaphorin receptor involved in the migration of activated B cells (Holl et al., 2011), and CXCR7, a CXCL12 receptor which promotes B cell localization and retention in the MZ (Wang et al., 2012), were up-regulated in IRF4-deficient B cells. The differential expression of these genes was confirmed by quantitative RT-PCR (qRT-PCR; Fig. 3 B). The results were confirmed by flow cytometric analysis for ALCAM and CXCR7, for which antibodies were available (Fig. 3 C).

In the stringent supervised analysis, genes differentially expressed between *irf4*$^{-/-}$ and *irf4*$^{+/+}$ B cells at a lower fold difference may have escaped detection. To further explore the molecular basis for the accumulation of *irf4*-deleted B cells in the MZ, we therefore analyzed the expression pattern of molecules known to regulate the positioning of B cells in the MZ. First, we performed flow cytometric analysis for the integrins $\alpha_L\beta_2$ (LFA-1) and $\alpha_4\beta_1$ (VLA-4), which are expressed at elevated levels on MZ B cells, mediating their retention in this microenvironment (Lu and Cyster, 2002). We found that the expression of integrin chains α_L and β_1 was increased on IRF4-deficient MZ and FO B cells compared with their wild-type counterparts (Fig. 4 A); α_4 expression was up-regulated on the cell surface of MZ B cells from *irf4*$^{-/-}$ versus *irf4*$^{+/+}$ mice (Fig. 4 A). The elevated expression of these integrin chains on the cell surface of IRF4-deficient B cells may promote their retention in the MZ by increasing the adhesiveness of these cells through binding to their respective ligands, as described previously (Lu and Cyster, 2002). Second, we determined the mRNA expression levels of cannabinoid receptor 2 (CB2; Muppidi et al., 2011) and sphingosine-1-phosphate receptors 1 and 3 ($S1P_1$ and $S1P_3$; Cinamon et al., 2004; Cyster and Schwab, 2012), which are involved in the positioning of B cells in the MZ. We did not detect differences in CB2 and $S1P_1$ transcript levels between *irf4*$^{-/-}$ and *irf4*$^{+/+}$ B cells (not depicted). Conversely, $S1P_3$ mRNA was 2.3-fold up-regulated in IRF4-deficient versus wild-type B cells (Fig. 4 B). We were unable to determine $S1P_3$ cell surface expression because of the lack of a suitable reagent. However, the elevated expression of $S1P_3$ mRNA in IRF4-deficient B cells would predict increased chemotaxis to sphingosine-1-phosphate (S1P). We therefore assessed the migratory response of *irf4*$^{-/-}$ and *irf4*$^{+/+}$ B cells to S1P in a transwell assay and found that IRF4-deficient FO and MZ B cells showed a significantly increased chemotactic response compared with

was calculated using the ImageJ software on three mice of each genotype from three independent experiments (+/+: 24 follicles; fl/+: 33 follicles; fl/fl: 25 follicles). Data are shown as mean ± SD. Statistical significance was determined by Student's t test (**, $P < 0.01$). (D) IgM expression in splenic sections of CD20-TAM-Cre, *irf4*$^{fl/+}$CD20-TAM-Cre, and *irf4*$^{fl/fl}$CD20-TAM-Cre mice was assessed by IHC. Boxes demarcate the area shown at higher magnification below. (B and D) Dashed lines demarcate the border between the FO and MZ areas. (E) IgD and IgM expression in the spleen of CD20-TAM-Cre, *irf4*$^{fl/+}$CD20-TAM-Cre, and *irf4*$^{fl/fl}$CD20-TAM-Cre mice was analyzed by IHC. Dashed lines mark the inner and outer border of the MZ area. Bars: (B [left] and D [top]) 500 µm; (B, right) 125 µm; (D [bottom] and E) 100 µm.

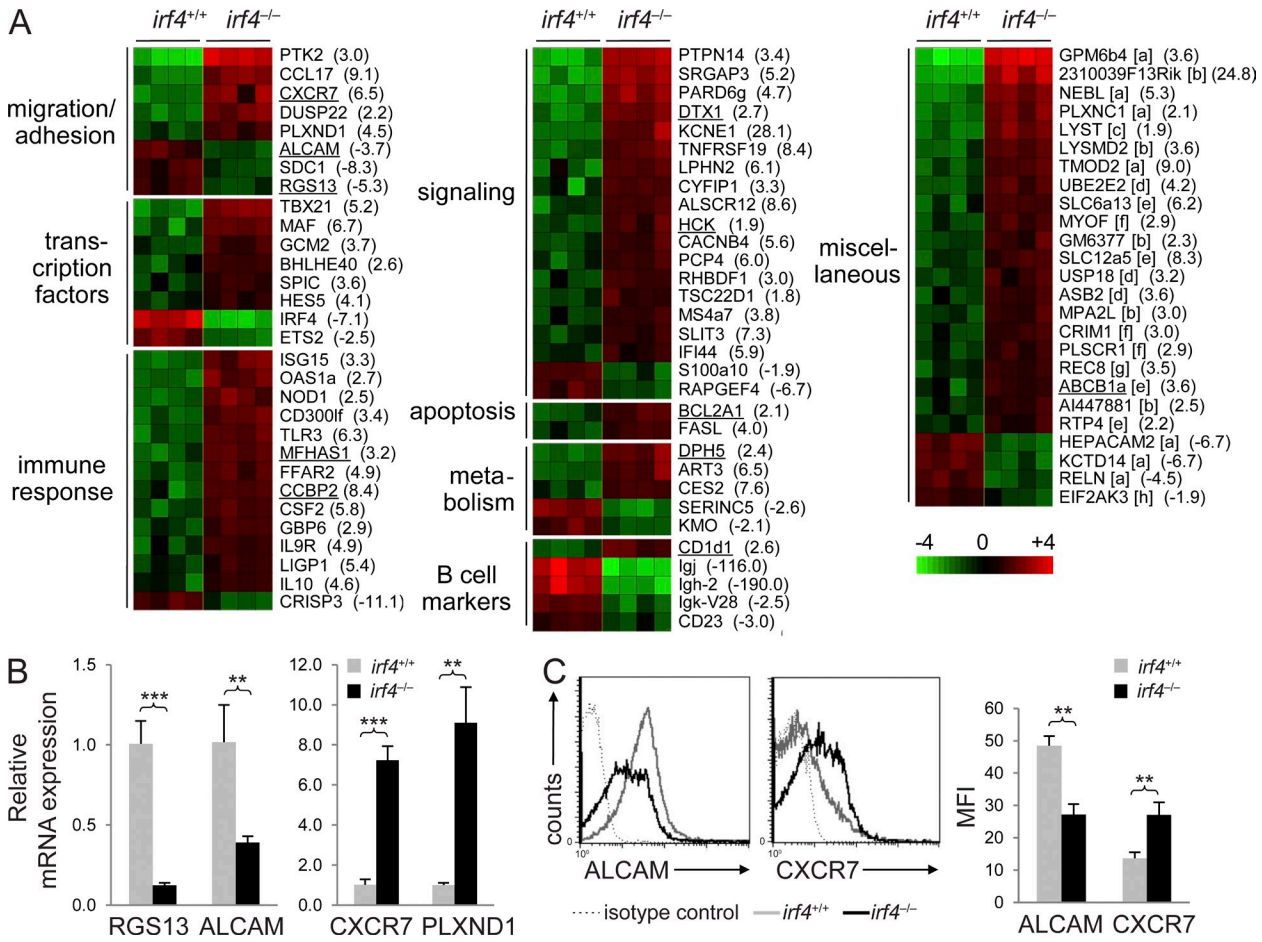

Figure 3. GEP analysis of IRF4-deficient and wild-type B cells. (A) RNA was isolated from splenic *irf4*$^{-/-}$ and *irf4*$^{+/+}$ B cells purified by magnetic cell separation and processed for hybridization on microarrays arrays (B cell fractions were isolated separately from four mice per genotype and independently processed for microarray hybridization). Gene expression differences between *irf4*$^{+/+}$ and *irf4*$^{-/-}$ B cells were determined by supervised analysis (n = 4 each group). Color changes within a row indicate expression levels relative to the mean of the sample population. Values are quantified by the scale bar that visualizes the difference in the z_{ge} score (expression difference/SD) relative to the mean (0). Genes are ranked according to their z_g score (mean expression difference of the respective gene between IRF4-deficient and wild-type samples/SD). The gene expression differences among the genotypes are shown in brackets and grouped according to functional or operational categories: [a] cytoskeleton/membrane function, [b] unknown, [c] cellular trafficking, [d] protein degradation, [e] transporter protein, [f] cell membrane protein, [g] metabolism, and [h] translation. Genes that showed the same trend of expression compared with a published GEP analysis of MZ versus FO B cells are underlined. (B) Total RNA from *irf4*$^{+/+}$ and *irf4*$^{-/-}$ splenic B cells was analyzed for expression of RGS13, ALCAM, CXCR7, and PLXND1 by qRT-PCR. The expression was corrected for β-actin levels and then normalized to wild-type B cells. Data are shown as mean ± SD (n = 3, two independent experiments). Statistical significance was analyzed by Student's t test (**, $P < 0.01$; ***, $P < 0.001$). (C) ALCAM and CXCR7 expression on IgM$^+$ splenic B cells from *irf4*$^{+/+}$ and *irf4*$^{-/-}$ mice was assessed by flow cytometry. Data are shown as mean ± SD (n = 6, two independent experiments). Statistical significance was determined by Student's t test (**, $P < 0.01$).

the corresponding wild-type B cell subsets (3.0- or 2.3-fold increase over wild-type at 100 nM S1P, respectively; Fig. 4 C). The results suggest that deletion of *irf4* promotes the migration of B cells to the MZ in response to S1P. Collectively, the differential expression of genes with functions in cell trafficking and adhesion in the mature IRF4-deficient B cells may provide an explanation for their altered migratory and homing properties.

IRF4-deficient B cells show increased activation of the NOTCH2 pathway

The GEP analysis also revealed a significant up-regulation of the NOTCH target genes *hes5* and *dtx1* (Saito et al., 2003) in the IRF4-deficient as compared with wild-type B cells (4.1- and 2.7-fold, respectively; Fig. 3 A), which was confirmed by qRT-PCR (5.2- and 2.4-fold; Fig. 5 A). This finding was indicative of increased activation of the NOTCH pathway in *irf4*$^{-/-}$ B cells and prompted us to examine the expression and activation status of NOTCH receptors in those cells. mRNA encoding NOTCH3 and NOTCH4 was not detectable in *irf4*$^{-/-}$ and *irf4*$^{+/+}$ B cells (not depicted), and no significant differences in the mRNA levels of NOTCH1 or the amount of the active form of NOTCH1 protein (not depicted) were observed among the genotypes. However, Western blot analysis showed that NOTCH2 protein expression was strongly

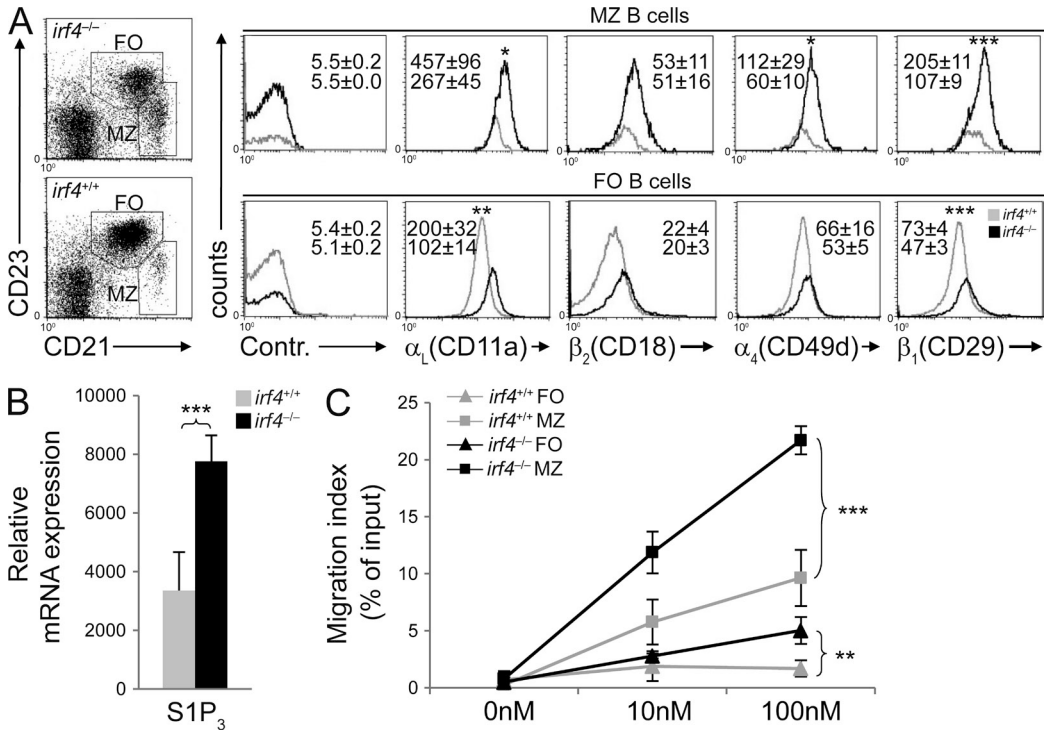

Figure 4. Analysis for the expression of molecules associated with MZ localization on B cells of IRF4-deficient and wild-type mice. (A) Expression of integrins α_L, β_2, α_4, and β_1 on MZ and FO B cells from *irf4*$^{+/+}$ and *irf4*$^{-/-}$ mice was assessed by flow cytometry. MZ and FO gates are indicated on the corresponding dot plots. Numbers on plot (top, *irf4*$^{-/-}$; bottom, *irf4*$^{+/+}$) show average mean fluorescence intensity (MFI) value ± SD (n = 3, two independent experiments). Statistical significance was determined by Student's t test (*, P < 0.05; **, P < 0.01; ***, P < 0.001). (B) $S1P_3$ expression in *irf4*$^{+/+}$ and *irf4*$^{-/-}$ splenic B cells was assessed by GEP. Data are shown as mean ± SD (n = 4, as in Fig. 3 A). Statistical significance was determined by Student's t test (***, P < 0.001). (C) The chemotactic response of *irf4*$^{+/+}$ and *irf4*$^{-/-}$ MZ and FO B cells to S1P was determined by enumerating splenic cells transmigrated for 3 h across uncoated 5-µm transwells to S1P or media and by analyzing them for CD19, CD21, and CD23 expression by flow cytometry. Chemotactic response is presented as migration index (percentage of input cells that migrated to the lower chamber). Data represent mean ± SD (n = 3 for 0 and 100 nM; n = 2 for 10 nM; three independent experiments). Statistical significance is shown for results obtained with 100 nM S1P and was determined by Student's t test (**, P < 0.01; ***, P < 0.001).

up-regulated in *irf4*$^{-/-}$ versus wild-type B cells (Fig. 5 B; the band at 80 kD is likely to be unspecific), and flow cytometric analysis demonstrated increased cell surface expression of NOTCH2 on both FO and MZ B cell subsets of *irf4*$^{-/-}$ compared with *irf4*$^{+/+}$ mice (Fig. 5 C). The elevated amounts of NOTCH2 protein in *irf4*$^{-/-}$ B cells are not caused by changes in transcriptional activation because IRF4-deficient and wild-type B cells expressed similar amounts of NOTCH2 mRNA (Fig. 5 D), suggesting the existence of posttranscriptional mechanisms.

We then determined the activation status of NOTCH2 in B cells from *irf4*$^{-/-}$ and *irf4*$^{+/+}$ mice by analyzing nuclear translocation of NOTCH2 (Fig. 5, E and F). Western blot analysis of *irf4*$^{-/-}$ and *irf4*$^{+/+}$ B cells revealed an increase in the expression of both cytosolic/membranous NOTCH2 (the band above 250 kD in the C + M fraction is consistent with the 300-kD NOTCH2 precursor) and nuclear (i.e., active) NOTCH2 in IRF4-deficient compared with wild-type splenic B cells (Fig. 5 E). Of note, a lower molecular weight band was visualized by the α-NOTCH2 antibody in the nuclear fractions but not in the cytosolic/membranous fractions, consistent with the NOTCH2-intracellular (IC) domain that translocates to the nucleus upon proteolytic cleavage. These data indicate that *irf4*$^{-/-}$ B cells have enhanced activation of NOTCH2, likely caused by the presence of an increased number of B cells expressing nuclear NOTCH2 in the spleen of *irf4*$^{-/-}$ compared with wild-type mice (Fig. 5 F).

To determine whether the accumulation of *irf4*-deleted B cells in the MZ of *irf4*$^{fl/fl}$CD20-TAM-Cre mice (see Fig. 2, B–E) is associated with the activation of the NOTCH2 pathway, we analyzed spleen sections for nuclear translocation of NOTCH2. We observed that the majority of B cells in the MZ area of *irf4*$^{fl/fl}$CD20-TAM-Cre mice displayed nuclear NOTCH2 (Fig. 5 G), demonstrating that NOTCH2 is indeed activated in these cells. Flow cytometric analysis detected up-regulation of NOTCH2 surface expression on eGFP$^+$ MZ B cells from *irf4*$^{fl/fl}$CD20-TAM-Cre versus *irf4*$^{fl/+}$CD20-TAM-Cre mice (Fig. 5 H). The data suggest that in the absence of IRF4, enhanced activation of NOTCH2, a known regulator of MZ B cell development (Saito et al., 2003; Hampel et al., 2011), may causally contribute to the altered migration/homing properties of B cells that are reflected by their retention in the MZ.

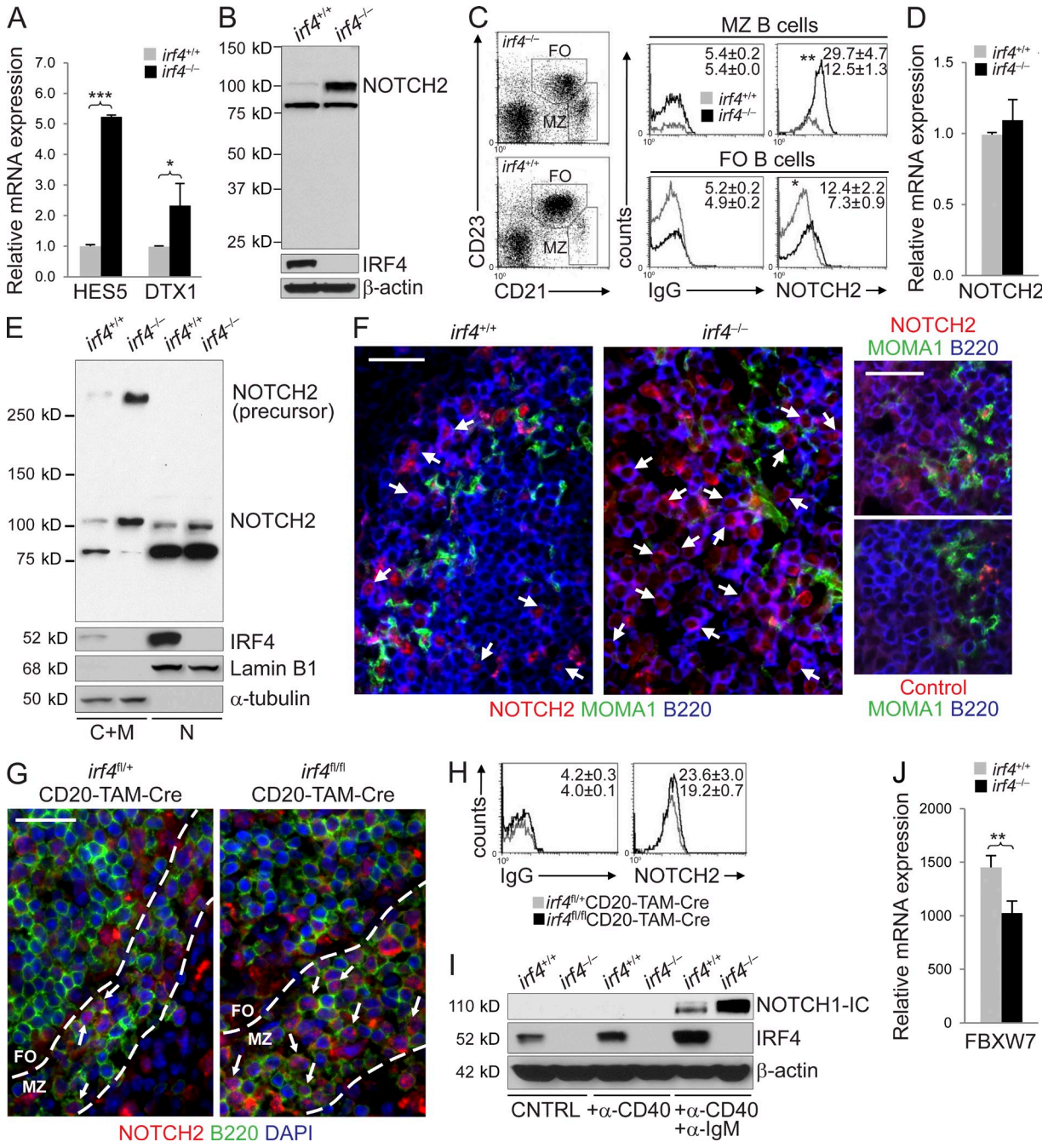

Figure 5. Elevated activation of the NOTCH pathway in IRF4–deficient B cells. (A) *irf4*$^{+/+}$ and *irf4*$^{-/-}$ splenic B cells were analyzed for expression of HES5 and DTX1 by qRT-PCR. The expression was corrected for β-actin levels and then normalized to wild-type B cells. Data are shown as mean ± SD ($n = 3$). Statistical significance was determined by Student's *t* test (*, $P < 0.05$; ***, $P < 0.001$). (B) NOTCH2 expression in *irf4*$^{+/+}$ and *irf4*$^{-/-}$ splenic B cells was analyzed by Western blot (whole cell lysates; one representative of three independent experiments). (C) NOTCH2 expression on MZ and FO B cells from *irf4*$^{+/+}$ and *irf4*$^{-/-}$ mice was analyzed by flow cytometry (gates are indicated on the corresponding dot plots). Data are shown as average mean fluorescence intensity (MFI) value ± SD ($n = 3$; top, *irf4*$^{-/-}$; bottom, *irf4*$^{+/+}$). Statistical significance was determined by Student's *t* test (*, $P < 0.05$; **, $P < 0.01$). (D) NOTCH2 mRNA expression in *irf4*$^{+/+}$ and *irf4*$^{-/-}$ splenic B cells was analyzed by qRT-PCR as described in A. Data are shown as mean ± SD ($n = 3$). (E) NOTCH2 protein expression in the cytosolic/membranous (C + M) and nuclear (N) protein fractions of *irf4*$^{+/+}$ and *irf4*$^{-/-}$ B cells was determined by Western blot (one representative of two independent experiments). Lamin B1 and α-tubulin were used as loading controls for N and C + M fractions, respectively. (F) NOTCH2, MOMA1, and B220 expression in spleen sections from *irf4*$^{+/+}$ and *irf4*$^{-/-}$ mice was analyzed by IF. Arrows indicate B220^{+} B cells expressing nuclear NOTCH2. One representative mouse out of four per group is shown. (right) Specificity of the NOTCH2 staining was confirmed by isotype control staining on consecutive sections. (G) NOTCH2 and B220 expression in the spleen of *irf4*$^{fl/fl}$CD20-TAM-Cre and *irf4*$^{fl/+}$CD20-TAM-Cre mice was analyzed by IF. Nuclei were stained with DAPI. Dashed lines mark the inner and outer border of the MZ area. Arrows indicate B220^{+} B cells expressing nuclear NOTCH2. One representative mouse per group

IRF4 exerts a suppressive function on the NOTCH pathway also in activated B cells

Our findings suggest that IRF4 represses activation of the NOTCH2 pathway in quiescent mature B cells in vivo. Previous studies reported up-regulation of the NOTCH target gene *hes1* in B cells upon BCR-mediated stimulation in vitro (Nie et al., 2003) and synergism between NOTCH and BCR signaling (Thomas et al., 2007). To investigate whether IRF4 exerts a suppressive function on the NOTCH pathway also in activated B cells, we studied the relationship between IRF4 and NOTCH activation in *irf4*$^{-/-}$ and *irf4*$^{+/+}$ B cells upon stimulation with signals that mimic α-IgM and α-CD40 activation (stimulation through the CD40 receptor was required during culturing to rescue *irf4*$^{-/-}$ B cells from α-IgM–induced cell death [Mittrücker et al., 1997]). Poor activation of NOTCH2 was observed in either genotype (not depicted). However, combined α-IgM and α-CD40 treatment induced activation of NOTCH1 in both *irf4*$^{+/+}$ and *irf4*$^{-/-}$ B cells, with a dramatically increased amount of the active form of NOTCH1 protein (NOTCH1-IC) in the IRF4-deficient relative to wild-type B cells (Fig. 5 I). In contrast, NOTCH1-IC was not detectable in B cells cultured in medium only, and CD40 stimulation alone did not induce NOTCH1 activation (Fig. 5 I). These findings reveal that BCR stimulation activates NOTCH1 and provide evidence that IRF4 down-modulates NOTCH1 signaling in activated B cells.

We then looked for possible posttranscriptional mechanisms that may account for the elevated amounts of NOTCH proteins in IRF4-deficient B cells. We did not observe down-regulation of microRNAs known or predicted to regulate NOTCH expression (including members of miR-34, miR-181, miR-107, miR-9, and miR-18 families) among *irf4*$^{-/-}$ and wild-type B cells (not depicted), arguing against a microRNA-associated dysregulation of NOTCH expression in IRF4-deficient B cells. The ubiquitin ligase FBXW7 targets NOTCH for proteasomal degradation (Aifantis et al., 2008; Welcker and Clurman, 2008). We observed ∼30% reduction of FBXW7 mRNA levels in *irf4*$^{-/-}$ versus *irf4*$^{+/+}$ B cells (Fig. 5 J); however, we were unable to quantify FBXW7 protein levels in those cells, as suitable reagents are not yet available. In summary, we observed that IRF4 deficiency was associated with enhanced NOTCH2 and NOTCH1 activation in quiescent and BCR-stimulated B cells, respectively, suggesting a general role for IRF4 in the repression of the NOTCH pathway in mature B cells.

Retention of IRF4-deficient B cells in the MZ is dependent on NOTCH2 signaling

To determine whether the accumulation of *irf4*-deleted B cells in the MZ of *irf4*$^{fl/fl}$CD20-TAM-Cre mice (see Fig. 2, B–E) is dependent on the activation of the NOTCH2 pathway (see Fig. 5, E–G), we analyzed the topography of the MZ and FO areas in mice where the activation of NOTCH2 was inhibited in vivo by administration of a therapeutic monoclonal antibody that stabilizes the quiescent conformation of the negative regulatory region of NOTCH2 (anti–negative regulatory region 2 antibody [α-NRR2; Wu et al., 2010]). We administered α-NRR2 as a single dose at day 11 after the last TAM injection, i.e., when IRF4-deficient B cells have already accumulated in the MZ. The results showed that within 72 h, α-NRR2 effectively reverted the accumulation of B cells in the MZ of *irf4*$^{fl/fl}$CD20-TAM-Cre mice, whereas treatment with an irrelevant isotype-matched antibody had no effect (Fig. 6 A).

To determine whether the α-NRR2–induced dissolution of the MZ in *irf4*$^{fl/fl}$CD20-TAM-Cre mice was caused by the mobilization as opposed to the disappearance of *irf4*-deleted B cells, we performed flow cytometric analysis of splenic B cells for eGFP in combination with B cell markers discriminating MZ and FO B cells. We observed that both eGFP^{+} and eGFP^{-} CD21^{hi}CD23^{-} MZ B cells were depleted from the spleen after α-NRR2 administration, whereas the fractions of CD21^{int}CD23^{+} FO B cells showed no significant differences among the genotypes and between α-NRR2 and control antibody treatment (Fig. 6 B and Table 2). Specifically, the percentage of eGFP^{+} B cells was not significantly reduced after α-NRR2 treatment in both *irf4*$^{fl/fl}$CD20-TAM-Cre and *irf4*$^{fl/+}$CD20-TAM-Cre mice. In addition, FO B cells were detectable at comparable fractions in both genotypes, and the percentages of eGFP^{+} FO B cells did not differ significantly among the *irf4*$^{fl/fl}$CD20-TAM-Cre and *irf4*$^{fl/+}$CD20-TAM-Cre mice upon α-NRR2 and control antibody treatment (Fig. 6 B and Table 2). Thus, the α-NRR2 treatment did not affect the fraction of *irf4*-deleted FO B cells in the spleen, suggesting that the cells relocalized from the MZ to the FO area.

In summary, these data show that MZ B cells, independent of their *irf4* deletion status, were depleted from the spleen, whereas *irf4*-deleted FO B cells underwent relocalization within the splenic microenvironment, presumably by trafficking back to the FO area. The ability of NOTCH2 inhibition to displace B cells from the MZ after they have accumulated suggests that B cells require continuous, active NOTCH2 signaling for their retention in the MZ area.

is shown (*irf4*$^{fl/fl}$CD20-TAM-Cre: $n = 6$; *irf4*$^{fl/+}$CD20-TAM-Cre: $n = 8$; four independent experiments). (F and G) Bars, 50 µm. (H) NOTCH2 expression on eGFP^{+} MZ B cells of *irf4*$^{fl/fl}$CD20-TAM-Cre and *irf4*$^{fl/+}$CD20-TAM-Cre mice was analyzed by flow cytometry. Values on plot indicate average MFI value ± SD ($n = 3$–4, two independent experiments; top, *irf4*$^{fl/fl}$; bottom, *irf4*$^{fl/+}$). The statistical significance was determined to be $P = 0.06$ by Student's *t* test. (I) *irf4*$^{+/+}$ and *irf4*$^{-/-}$ splenic B cells were stimulated with α-CD40 alone or in combination with α-IgM for 48 h, and NOTCH1 activation was assessed by Western blot. Control cells (CNTRL) were cultured for 4 h in medium only. The figure shows one representative of three independent experiments. (J) FBXW7 expression in *irf4*$^{+/+}$ and *irf4*$^{-/-}$ splenic B cells was assessed by GEP. Data are shown as mean ± SD ($n = 4$). Statistical significance was determined by Student's *t* test (**, $P < 0.01$).

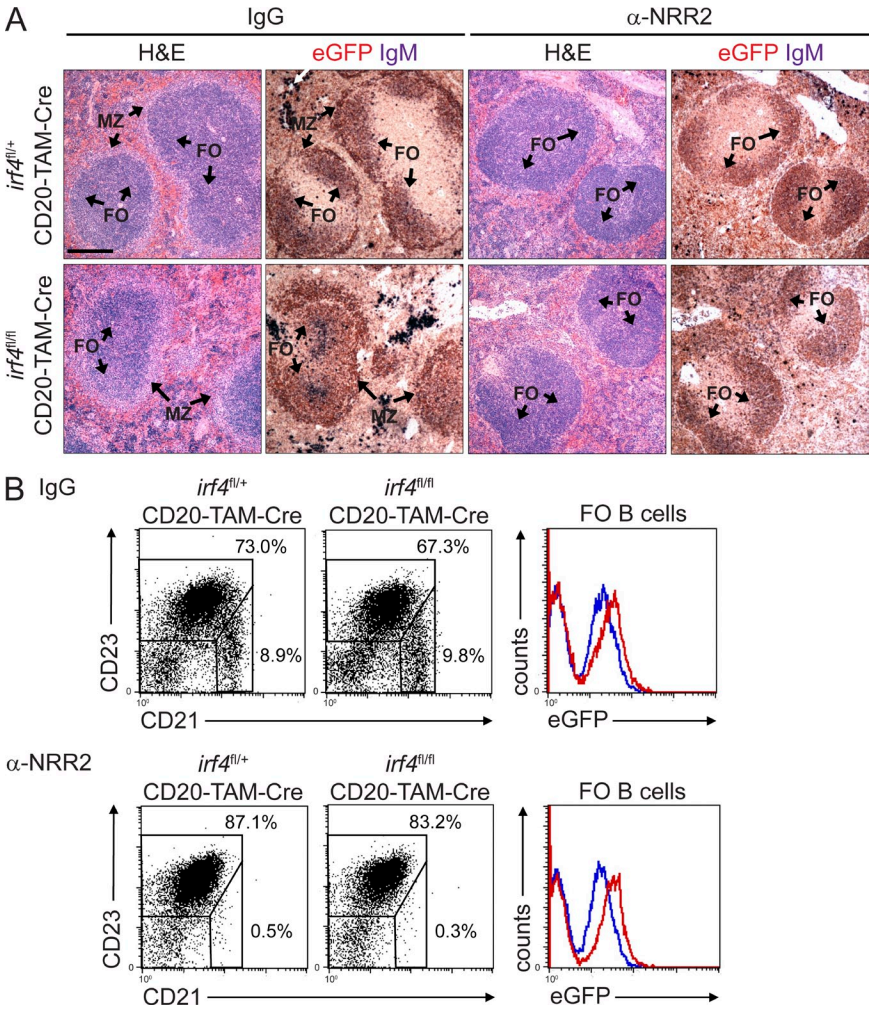

Figure 6. Disappearance of B cells from the MZ of *irf4*$^{fl/fl}$CD20-TAM-Cre mice upon inhibition of NOTCH2 activation. *irf4*$^{fl/+}$CD20-TAM-Cre and *irf4*$^{fl/fl}$CD20-TAM-Cre mice were treated with TAM (days 0–2) followed by a single dose of α-NRR2 (or IgG, day 13) and analyzed 72 h after antibody administration. Data show results from one representative mouse out of four (four independent experiments). (A) Spleen sections from *irf4*$^{fl/+}$CD20-TAM-Cre and *irf4*$^{fl/fl}$CD20-TAM-Cre mice were stained with H&E or analyzed for expression of eGFP and IgM after in vivo treatment with IgG or α-NRR2 antibody. Bar, 500 µm. (B) CD21 and CD23 expression by CD19^{+} splenic B cells of *irf4*$^{fl/+}$CD20-TAM-Cre and *irf4*$^{fl/fl}$CD20-TAM-Cre mice was assessed by flow cytometry after in vivo treatment with IgG or α-NRR2 antibodies. Numbers above gates indicate percentage of CD23^{+}CD21^{int} FO and CD23^{-}CD21^{hi} MZ B cells. Right plots show histogram of eGFP expression by splenic FO B cells of *irf4*$^{fl/+}$CD20-TAM-Cre (blue lines) and *irf4*$^{fl/fl}$CD20-TAM-Cre (red lines) mice.

To investigate whether α-NRR2–induced dissolution of the MZ is indeed causally linked with inhibition of NOTCH2 activation in B cells, we determined the NOTCH2 activation status in B cells of α-NRR2–treated *irf4*$^{-/-}$ mice in the MZ area shortly after antibody administration (12 and 24 h; Fig. 7 A). The results showed that inhibition of NOTCH2 activation induced a dramatic decrease of nuclear NOTCH2 localization in B cells as early as 12 h, which was not observed in the IgG control treatment (Fig. 7 A). Thus, the dissolution of the MZ is preceded by the inhibition of NOTCH2 signaling in B cells.

Continued NOTCH2 signaling is required for the retention of B cells in the MZ area

The observation that NOTCH2 activation was rapidly inhibited upon α-NRR2 treatment (Fig. 7 A) and that the MZ area was entirely devoid of B cells 72 h after a single α-NRR2 injection (Fig. 6 A) led us to determine the kinetics of α-NRR2–induced MZ dissolution within the 12–72 h time window. Flow cytometric analysis of spleens from wild-type mice treated with α-NRR2 showed a progressive decrease in the percentage of MZ B cells, reaching 50% depletion 24–36 h after treatment and a complete depletion between 48 and 72 h (Fig. 7 B, top). In accordance, IHC analysis revealed that the MZ B cell rim showed a progressive disruption (see 24-h time point) until becoming almost undetectable at 48 h (Fig. 7 C).

To elucidate the basis for the disappearance of MZ B cells upon α-NRR2 treatment, we first assessed by TUNEL staining (that detects apoptosis-associated DNA fragmentation) whether treated mice showed in situ cell death of MZ B cells at time points 24, 36, and 48 h. We observed only rare TUNEL^{+}IgM^{+} B cells in the MZ area after α-NRR2 administration, similar to IgG-treated controls (not depicted), indicating that in situ cell death of α-NRR2–treated MZ B cells within the MZ does not represent the major mechanism for their disappearance. To determine whether α-NRR2–treated MZ B cells may egress into the peripheral blood, we analyzed the circulating B cell compartment of treated and control mice within a 12–72-h time window (Fig. 7 B, bottom). The results showed that B cells with a MZ B cell immunophenotype were transiently detectable in the blood of treated mice, peaking at ∼2.4% ($P < 0.01$) of peripheral blood B cells 36 h after antibody administration

Table 2. Frequencies of eGFP+ and FO B cells in the spleen of *irf4*^{floxed}CD20-TAM-Cre mice 72 h after α-NRR2 treatment

Genotype	Treatment	% eGFP+CD19+ cells	% FO (among CD19+ cells)	% eGFP+ B cells (among FO)
irf4$^{fl/+}$CD20-TAM-Cre	IgG (*n* = 4)	51.4 ± 2.6	76.4 ± 3.6	54.9 ± 2.9
	α-NRR2 (*n* = 4)	44.0 ± 6.0	88.1 ± 3.0	48.3 ± 5.8
irf4$^{fl/fl}$CD20-TAM-Cre	IgG (*n* = 4)	59.1 ± 11.7	73.9 ± 5.2	62.0 ± 10.4
	α-NRR2 (*n* = 4)	49.6 ± 4.8	85.3 ± 3.0	55.4 ± 4.8

before reaching pretreatment levels of ∼1% at 72 h (Fig. 7 B). Those cells may be quickly cleared from the circulation by phagocytic macrophages as described for GC B cell death and for glucocorticoid-induced thymocyte death (Nakamura et al., 1996, 1997). Alternatively, the cells may have aberrantly lodged in other organs or changed their immunophenotype. However, whereas it has been firmly established that MZ B cells can be replenished from FO-type B cells (Pillai and Cariappa, 2009), there is no evidence for a similar plasticity of MZ B cells.

DISCUSSION

Here we identified a novel biological function for the transcription factor IRF4 in the homeostasis of the mature B cell repertoire and in the regulation of the NOTCH pathway. We found that inducible deletion of *irf4* in quiescent mature B cells led to aberrant accumulation of FO B cells in the MZ area. The retention of *irf4*-deficient B cells in the MZ was associated with elevated protein expression and activation of NOTCH2. Inhibition of NOTCH2 activation in vivo with a NOTCH2-inhibitory antibody reversed the aberrant accumulation of FO B cells in the MZ area. In addition, we observed that MZ B cells rapidly disappeared from the spleen and peripheral blood within a few days after NOTCH-inhibitory antibody administration. Our results identify a previously unrecognized role for IRF4 in quiescent mature B cells in addition to providing new insights into the dependence of MZ B cells on NOTCH2 signaling.

Deletion of *irf4* leads to the accumulation of FO B cells in the MZ area. IRF4 may control B cell positioning by regulating the expression of genes that have been associated with the trafficking of MZ B cells, including ALCAM/CD166, CXCR7, integrin chains α_L and β_1, and $S1P_3$ receptor. Moreover, the morphology of the white pulp and the dynamics of MZ and FO B cell movements (Arnon et al., 2013) provide a conceivable explanation for the accumulation of *irf4*-deleted FO B cells in the MZ area as the result of aberrant NOTCH2 activation. The MZ is the site of entry and egress of cells from the spleen. FO B cells transit from the follicle to the MZ and are released through the red pulp into the bloodstream because of their low capacity to adhere to stromal cells (Arnon et al., 2013). Recirculating FO B cells exit the bloodstream through fenestrations in the red pulp venules; however, unlike MZ B cell precursors, FO B cells may be insensitive to DLL1-mediated signaling and move across the marginal sinus into the follicle (Pillai and Cariappa, 2009) at a surprisingly high rate (Arnon et al., 2013). The aberrantly elevated levels of NOTCH2 protein in IRF4-deficient FO B cells may lead to DLL1-mediated activation of NOTCH2 signaling that is sufficient to temporarily retain those cells in the MZ during their entry or egress from the spleen. The importance of NOTCH2 signaling in this process is demonstrated by the rapid egress of these cells from the MZ area upon inhibition of NOTCH2 activation. It is possible that similar to the FO B cells, deletion of *irf4* in MZ B cells of *irf4*$^{fl/fl}$CD20-TAM-Cre mice could lead to an increased MZ accumulation also of those cells because in normal mice, a sizable fraction of MZ B cells temporarily localize in the FO area while shuttling back and forth between the zones (Cinamon et al., 2008; Arnon et al., 2013). The precise mechanism of how IRF4 down-modulates NOTCH2 activation requires further study, although our results indicate a post-transcriptional regulatory mechanism.

Genetic manipulation in mouse models has firmly established a role for NOTCH2 in the generation of MZ B cells (Saito et al., 2003; Hampel et al., 2011). Initial evidence that NOTCH2 signaling may also be required for the maintenance of MZ B cells stems from two observations. First, treatment of mice with an anti-DLL1 antibody that blocks the NOTCH2-DLL1 interaction led to a gradual depletion of MZ B cells from the spleen ultimately showing a fivefold reduction in MZ B cell numbers after 4 wk (Moriyama et al., 2008). A recent study using a different anti-DLL1 monoclonal antibody observed an almost complete absence of MZ B cells in the spleen after 14 d of treatment, whereas anti-DLL4 administration had no effect (Tran et al., 2013). Second, repeated injections of mice with a NOTCH2 inhibitory antibody over 2 wk led to the disappearance of preexisting MZ B cells from the spleen (Wu et al., 2010). Strikingly, we here found that NOTCH2 inhibition caused a rapid depletion of B cells from the MZ area that was detectable as early as 24 h after antibody treatment and virtually completed by 48 h. The rapid egress of MZ B cells was preceded by the inhibition of nuclear translocation of NOTCH2, drawing a causal link between active NOTCH2 signaling and the retention of B cells in the MZ.

The MZ egress was accompanied by a transient MZ B cell lymphocytosis in the peripheral blood. A rapid displacement of B cells from the MZ leading to a marked lymphocytosis in the blood has previously been observed shortly (3 h) after antibody-mediated inhibition of the integrins LFA-1 and $\alpha_4\beta_1$ that are required for MZ retention through ICAM-1– and VCAM-1–mediated adhesion (Lu and Cyster, 2002). We propose that NOTCH2 may control a biological

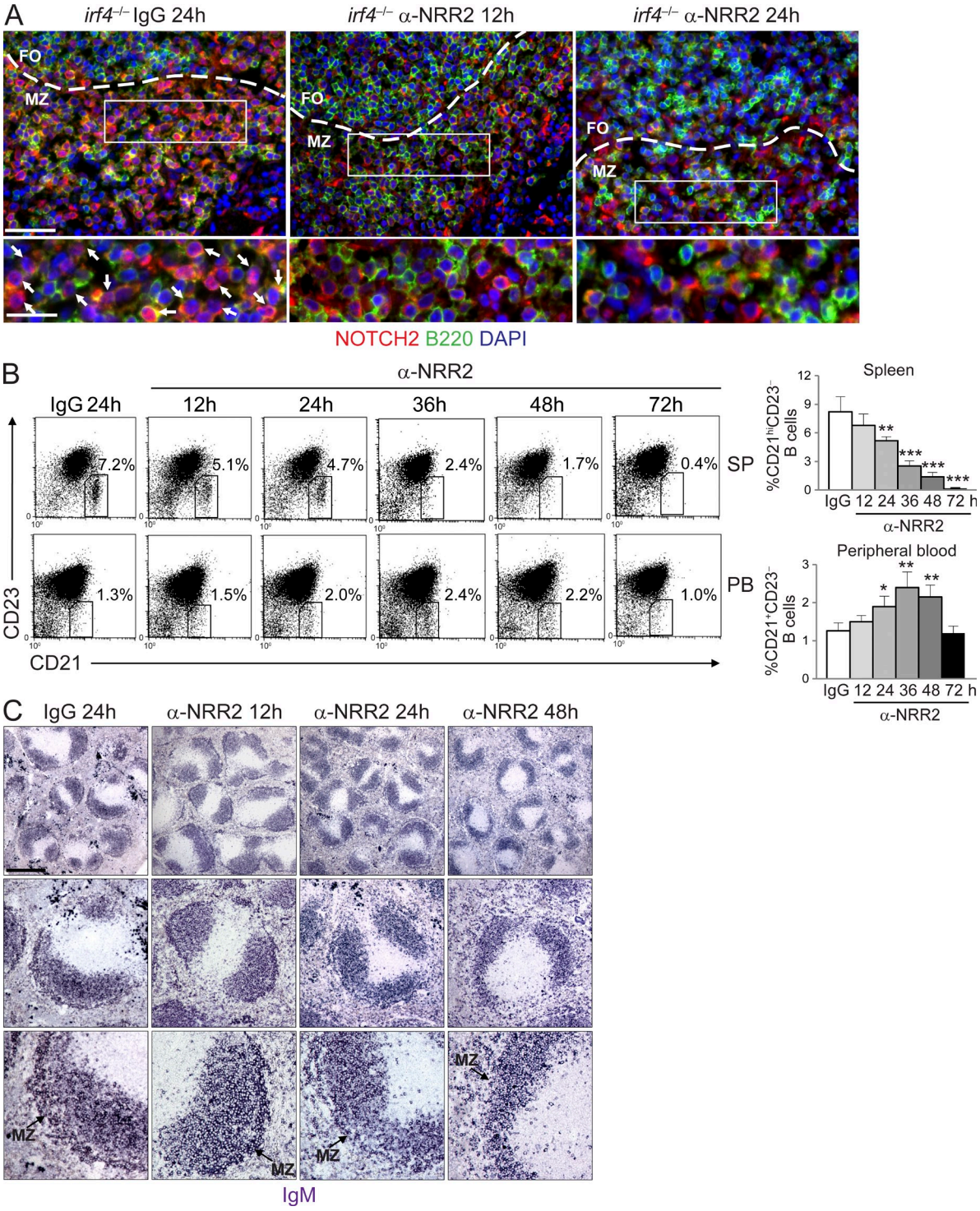

Figure 7. Rapid disruption of the splenic MZ area upon in vivo treatment with α–NRR2 antibody. (A) *irf4*$^{-/-}$ mice were injected with α-NRR2 (12 and 24 h) or IgG (24 h) antibodies, and NOTCH2 and B220 expression in spleen sections was assessed by IF. Nuclei were stained with DAPI. Dashed lines demarcate the border between the FO and MZ areas. Arrows indicate B220^{+} B cells expressing nuclear NOTCH2. One representative mouse out of two per group is shown (two independent experiments). Boxes demarcate the area shown below. (B) Wild-type mice were injected with α-NRR2 antibody (or IgG control), and CD21 and CD23 expression on CD19^{+} splenic (top) or peripheral blood (bottom) B cells was analyzed by flow cytometry at the indicated time points after antibody injection. Numbers above gates indicate percentage of CD23^{-}CD21$^{hi/+}$ B cells. Graphs show mean value ± SD of CD23^{-}CD21$^{hi/+}$ B cells in the spleen and in the peripheral blood of wild-type mice at the indicated time points (n = 4, four independent experiments). Statistical significance was analyzed by Student's t test (*, P < 0.05; **, P < 0.01; ***, P < 0.001). (C) Wild-type mice were treated as in B, and IgM expression in the spleen was assessed by IHC. One representative mouse out of four per group is shown (four independent experiments). Bars: (A, top) 100 µm; (A, bottom) 50 µm; (C, top) 1,000 µm; (C, middle) 400 µm; (C, bottom) 200 µm.

program that mediates the retention of B cells in the MZ. As a direct consequence of NOTCH2 inhibition, B cells may lose their adhesive properties and are flushed out of the MZ into the peripheral blood, as observed after integrin inhibition (Lu and Cyster, 2002). A further similarity between the NOTCH2 and integrin inhibition studies is the lack of detectable MZ B cells in the spleen and blood at day 3 or 4, respectively. We were unable to determine whether the rapid displacement of B cells from the MZ upon NOTCH2 inhibition was followed by cell death and eventual clearance of MZ B cells from the lymphoid system. However, our findings are compatible with the notion that the maintenance of MZ B cells may require positioning in the MZ microenvironment where the cells receive prosurvival signals from stromal cells.

Our findings may be relevant to the pathogenesis of mature B cell malignancies displaying dysregulated IRF4 and/or NOTCH activity. First, splenic MZ lymphoma (SMZL), a B cell malignancy of antigen-experienced B lymphocytes, has recently been demonstrated to carry recurrent mutations in the *NOTCH2* gene that lead to stabilization of the active form of the protein (Kiel et al., 2012; Rossi et al., 2012). Second, in CLL, *IRF4* is the susceptibility gene with the strongest risk association (Di Bernardo et al., 2008; Crowther-Swanepoel et al., 2010), and CLL cells are generally characterized by reduced IRF4 expression compared with normal B cells (Tsuboi et al., 2000; Brown et al., 2012; and GEP data published in Klein et al. [2001]). Of note, a recent study observed a relationship between low expression levels of IRF4 and the development of CLL in mice (Shukla et al., 2013). Third, CLL cells show constitutive activation of NOTCH1 and NOTCH2 receptors (Rosati et al., 2009, 2013) and stabilization of the active form of NOTCH1 caused by genetic alterations in a subset of cases (Fabbri et al., 2011; Puente et al., 2011). We here obtained evidence for BCR-associated NOTCH1 activation in mature B cells (Fig. 5 I). In the light of the recent demonstration of NOTCH1 recruitment to the immunological synapse after TCR activation (Guy et al., 2013), our results raise the possibility that also in B cells, NOTCH1 signaling may be activated via the antigen receptor. This may have implications for the pathogenesis of CLL, which is characterized by chronic BCR stimulation (Stevenson and Caligaris-Cappio, 2004). CLL cells are also dependent on the tumor microenvironment for their growth and survival (Ghia et al., 2008; Burger et al., 2009). Based on our in vivo results, we propose that alterations in the balance of the transcriptional network established by IRF4 and NOTCH2 may disrupt the normal migration and homing properties of B cells and thereby lead to aberrant positioning of the transformed CLL B cells in a lymphoid microenvironment that supports survival. In line with this notion, a pathogenic role for the aberrant retention of CLL cells in the lymphoid organs is strongly implied by the recent findings that BCR inhibitors work in part via tissue mobilization of CLL cells (Hoellenriegel et al., 2011; Ponader et al., 2012). In SMZL, the stabilized active form of NOTCH2 may favor the accumulation and retention of transformed B cells in the MZ. Interfering with NOTCH2 activation could mobilize the CLL and SMZL tumor cells from the lymphoid tissues and potentially increase the efficacy of chemotherapeutic agents.

MATERIALS AND METHODS

Mice. *irf4*$^{-/-}$ and *irf4*^{floxed} mice were generated as previously described (Klein et al., 2006) and backcrossed to C57BL/6 mice ($n > 10$). CD20-TAM-Cre mice (C57BL/6 background) were generated from a transgenic mouse line obtained by inserting an IRES-TAM-Cre cassette into the 3′ UTR of the hCD20 locus contained in the 158-kb BAC RP11-729B4 using homologous recombination (Khalil et al., 2012). Using a Rosa26-YFP reporter mouse, it was determined that 24 h after the final TAM administration (0.15 mg/g for three consecutive days; Sigma-Aldrich), 88% of B cells converted to YFP expression. Mice were housed and treated in compliance with the US Department of Health and Human Services Guide for the Care and Use of Laboratory Animals and according to the guidelines of the Institute of Comparative Medicine at Columbia University. The animal protocol was approved by the Institutional Animal Care and Use Committee of Columbia University.

Murine cell preparation. Spleen and peripheral blood were collected from mice and single-cell suspensions were subjected to hypotonic lysis. For in vitro experiments (cell culture, Western blot, and RNA isolation), CD19$^+$ B cells from spleen were enriched by magnetic depletion of non–B cells using the MACS B cell isolation kit (Miltenyi Biotec).

Flow cytometry. The following antibodies and labels were used on single-cell suspensions from mouse spleen and/or peripheral blood: peridinin chlorophyll protein cyanine 5.5–conjugated anti-CD19 (clone 1D3), FITC-conjugated anti-IgM, allophycocyanin-conjugated anti-CD21 (7G6), and PE-conjugated anti-CD23 (B3B4; all BD); PE-conjugated anti-CXCR7 and PE-conjugated anti-ALCAM (R&D Systems); and PE-conjugated anti-α_L (M17/4), PE-conjugated anti-α_4 (9C10), PE-conjugated anti-β_1 (HMβ1-1), PE-conjugated anti-β_2 (M18/2), PE-conjugated anti-NOTCH2 (HMN2-35), and the corresponding PE-conjugated isotype controls (all BioLegend). Data were acquired on a FACSCalibur (BD) using CELLQuest or CELLQuest Pro software (BD); data were analyzed using CELLQuest Pro. eGFP$^+$ B cells were isolated from the spleen by flow cytometry on a FACSAria (BD) after magnetic enrichment of B cells.

Immunofluorescence (IF). 3-µm-thick frozen sections were fixed with 4% paraformaldehyde. Nonspecific binding was blocked with 3% BSA in PBS solution plus 0.2% tween (PBST) or with 0.2% fish gelatin (for primary goat antibodies). Signal from endogenous biotin was blocked (avidin/biotin blocking kit; Vector Laboratories). Slides were incubated overnight with the following primary antibodies: biotin-conjugated anti-B220 (BD), rabbit anti-NOTCH2 (D76A6; Cell Signaling Technology) or rabbit IgG (Sigma-Aldrich), and goat anti–CD3-ε (M-20; Santa Cruz Biotechnology, Inc.). The slides were then washed and the following secondary antibodies were used: cyanin 3–conjugated anti–goat or anti–rabbit IgG (Jackson ImmunoResearch Laboratories, Inc.) and Alexa Fluor 350–conjugated or fluorescein-conjugated NeutrAvidin (Life Technologies). The sections were then either stained with FITC-conjugated anti-CD169 antibody (MOMA1; AbD Serotec) and mounted with Gold-Fade (Molecular Probes) or mounted and counterstained with DAPI (Molecular Probes). The images were acquired as monochromatic JPEG files by means of a Spot2 charge-coupled device camera (Diagnostic Instruments) mounted on an Eclipse E400 microscope (Nikon). The monochromatic images were merged in three-color images with Photoshop (Adobe Systems). Pictures were acquired using magnifications of 10, 20, and 40.

Histology and IHC. 3-µm-thick formalin-fixed, paraffin-embedded spleen sections were stained with hematoxylin and eosin (H&E). IHC was performed on paraffin-embedded sections except for the IgM/IgD staining

(frozen sections). Paraffin-embedded sections were dewaxed, antigen retrieved in 1 mM EDTA, and peroxidase inhibited as described previously (Ye et al., 1997; Cattoretti et al., 2005). Optimal cutting temperature compound (OCT)–embedded frozen sections were fixed with acetone. Endogenous HRP was quenched with 3% hydrogen peroxide solution and slides were blocked in 3% BSA in PBST plus 3% goat serum. The following primary antibodies were incubated overnight: anti-GFP rabbit antibody (Molecular Probes), anti–Ki-67 rabbit antibody (Thermo Fisher Scientific), and biotin-conjugated anti-IgD antibody (SouthernBiotech). Slides were then washed and counterstained with HRP-labeled anti–rabbit polymer (DAKO) or HRP-conjugated Streptavidin (Vector Laboratories), followed by AEC color development. Sections were counterstained with hematoxylin or stained with alkaline phosphatase–conjugated IgM antibody (SouthernBiotech), followed by development in nitro blue tetrazolium chloride–5-bromo-4-chloro-3-indolyl phosphate (NBT/BCIP; Roche). TUNEL staining was performed with the in situ cell death detection kit POD (Roche) according to manufacturer's instructions and followed by anti-IgM staining. The images were acquired by means of a Digital Sight camera (Nikon) mounted on an Eclipse E600 microscope (Nikon). Pictures were acquired using magnifications of 4, 10, 20, and 40. Quantitative analysis on images was performed using the ImageJ software (1.46r; National Institutes of Health) by measuring the mean ratio between the area of the splenic MZ and the lymphoid follicle.

GEP analysis. RNA was isolated using TRIzol (Invitrogen) from B cells purified by magnetic cell separation from *irf4*$^{-/-}$ and *irf4*$^{+/+}$ mice. Preparation of labeled cRNA was performed as described previously (Klein et al., 2001). Four independent samples of each genotype were hybridized to Mouse Genome 430 2.0 Arrays (Affymetrix) according to the manufacturer's recommendations. For supervised data analysis, we used a pattern discovery-based gene expression analysis tool as described previously (Klein et al., 2001). Microarray data are available through GEO accession no. GSE51932.

qRT-PCR. After TRIzol extraction, RNA was reverse transcribed into cDNA (Verso cDNA synthesis kit; Thermo Fisher Scientific). qRT-PCR was performed on the 7500 Real Time PCR System (Applied Biosystems) using the Absolute Blue QPCR Sybr low ROX Mix (Thermo Fisher Scientific). For primer sequences, see Table S1. Output data were analyzed with the SDS software (v1.4; Applied Biosystems). mRNA levels were normalized on the expression of β-actin, and wild-type B cells were used as calibrator sample. The results are presented as ratio between normalized expression of the gene of interest in the target and in the calibrator samples.

Chemotaxis assay. Splenic single-cell suspensions were subjected to red blood cell lysis and incubated for 40 min at 37°C in RPMI medium containing 10 mM Hepes and 2% fatty acid–free BSA in a water bath to desensitize. For chemotaxis assays, cells transmigrated for 3 h across uncoated 5-µm transwell filters (Corning) to S1P (Sigma-Aldrich) or media in the bottom chamber and were enumerated by collecting events for a fixed time (60 s) on a FACSCalibur. To determine the migration index of FO and MZ B cells, a fraction of cells recovered from the lower chamber was stained for CD19, CD21, and CD23 and analyzed by flow cytometry. Transwell assays were performed in duplicates or triplicates for each condition.

Cell lysis and Western blot analysis. Nuclear extracts were prepared according to a previously published protocol (Dominguez-Sola et al., 2007), with minor modifications. The cytosolic and membranous fraction was extracted upon incubation of the cells with 10 volumes of cytosol hypotonic buffer containing 0.5% NP-40 and spinning (1,500 rpm, 30 s; Eppendorf 5417R table-top centrifuge). The nuclear fraction was loaded on a 0.32 M sucrose solution to remove residues of membrane proteins and then washed in cytosol hypotonic buffer containing 0.5% NP-40. The nuclear pellet was resuspended in nuclear extraction buffer according to a previously published protocol (Dominguez-Sola et al., 2007). Whole cell lysate was prepared in NP-40–based lysis buffer. Protein extracts were resolved by SDS-PAGE and then electron-transferred onto nitrocellulose membranes. The following antibodies were used: rabbit anti-NOTCH2 (D67C8), rabbit anti–cleaved NOTCH1 (Val1744, D3B8), and rabbit anti–Lamin B1 (all Cell Signaling Technologies); rat anti-NOTCH2 (C651.6DbHn; Developmental Studies Hybridoma Bank); goat anti-IRF4 (M17; Santa Cruz Biotechnology); mouse anti–β-actin and mouse anti–α-Tubulin (Sigma-Aldrich); HRP-conjugated goat anti–rat IgG and HRP-conjugated anti–goat IgG (GE Healthcare); and HRP-conjugated goat anti–rabbit IgG and HRP-conjugated goat anti–mouse IgG (Thermo Fisher Scientific). ECL (GE Healthcare) and West-Dura reagents (Thermo Fisher Scientific) were used for detection.

B cell culture. B cells purified from the spleen of *irf4*$^{-/-}$ mice and wild-type littermates were cultured at a density of 10^6 cells/ml in RPMI medium plus 10% FBS and 2-mercaptoethanol for 48 h with 1 µg/ml anti–mouse CD40 (clone HM40-3; BD) with or without 15 µg/ml goat anti–mouse IgM F(ab′)2 fragments (Jackson ImmunoResearch Laboratories, Inc.).

In vivo inhibition of NOTCH2 activation. *irf4*^{floxed}CD20-TAM-Cre mice were injected i.p. with TAM and 15 mg/kg α-NRR2 (Wu et al., 2010) or IgG (Jackson ImmunoResearch Laboratories, Inc.) as control. We first confirmed that TAM injection did not interfere with the antibody activity and that we could successfully deplete MZ B cells in *irf4*$^{+/+}$CD20-TAM-Cre animals by administering three doses of α-NRR2 at days 10, 17, and 24 after TAM treatment (days 0–2) and analyzing the mice at day 27 (experimental setting from Wu et al. [2010]). *irf4*$^{fl/+}$CD20-TAM-Cre and *irf4*$^{fl/fl}$CD20-TAM-Cre mice received a single dose of α-NRR2, according to the following protocol: TAM days 0–2, α-NRR2 day 13, and analysis day 16. To study the mechanism of action of the α-NRR2 antibody, wild-type and *irf4*$^{-/-}$ mice were analyzed at short time points (12, 24, 36, 48 and 72 h) after injection of a single dose of α-NRR2.

Online supplemental material. Table S1 lists the primers used for qRT-PCR. Online supplemental material is available at http://www.jem.org/cgi/content/full/jem.20131026/DC1.

We thank Laura Pasqualucci for comments on the manuscript; David Dominguez-Sola, Jan Burger, Adolfo Ferrando, Boris Reizis, Riccardo Dalla-Favera, and Jeremy Samon for discussion; Jason Cyster for advice; Susan Schwab for advice on the chemotaxis assay, Łucja Grajkowska for technical help; Hongyan Tang and Qiong Shen for technical advice on staining procedures; and the Flow Cytometry, Genomics Technologies, Molecular Histology, and Confocal and Specialized Microscopy Shared Resources of the Herbert Irving Comprehensive Cancer Center (HICCC).

This work was supported by the HICCC, a grant from the CLL Global Research Foundation (USA), and National Cancer Institute/National Institutes of Health (NCI/NIH) grant R21-CA175461 to U. Klein, through fellowships of the Fondazione Cariplo (Italy) and the American–Italian Cancer Foundation (USA) to G. Simonetti and the German Research Council (DFG) to N. Heise, and a Cancer Biology Training Program fellowship (NCI/NIH grant 5T32-CA009503-26) to N.S. De Silva.

C.W. Siebel is employed by Genentech, which has commercial interests in the α-NRR2 antibody. The authors have no additional conflicting financial interests.

Submitted: 17 May 2013
Accepted: 19 November 2013

REFERENCES

Aifantis, I., E. Raetz, and S. Buonamici. 2008. Molecular pathogenesis of T-cell leukaemia and lymphoma. *Nat. Rev. Immunol.* 8:380–390. http://dx.doi.org/10.1038/nri2304

Arnon, T.I., R.M. Horton, I.L. Grigorova, and J.G. Cyster. 2013. Visualization of splenic marginal zone B-cell shuttling and follicular B-cell egress. *Nature.* 493:684–688.

Brown, J.R., M. Hanna, B. Tesar, N. Pochet, A. Vartanov, S.M. Fernandes, L. Werner, M. Ash, C.A. Roden, L. MacConaill, et al. 2012. Germline copy number variation associated with Mendelian inheritance of CLL in two families. *Leukemia.* 26:1710–1713. http://dx.doi.org/10.1038/leu.2012.33

Burger, J.A., P. Ghia, A. Rosenwald, and F. Caligaris-Cappio. 2009. The microenvironment in mature B-cell malignancies: a target for new treatment strategies. *Blood*. 114:3367–3375. http://dx.doi.org/10.1182/blood-2009-06-225326

Cattoretti, G., C. Angelin-Duclos, R. Shaknovich, H. Zhou, D. Wang, and B. Alobeid. 2005. PRDM1/Blimp-1 is expressed in human B-lymphocytes committed to the plasma cell lineage. *J. Pathol.* 206:76–86. http://dx.doi.org/10.1002/path.1752

Cattoretti, G., R. Shaknovich, P.M. Smith, H.M. Jäck, V.V. Murty, and B. Alobeid. 2006. Stages of germinal center transit are defined by B cell transcription factor coexpression and relative abundance. *J. Immunol.* 177:6930–6939.

Cayrol, R., K. Wosik, J.L. Berard, A. Dodelet-Devillers, I. Ifergan, H. Kebir, A.S. Haqqani, K. Kreymborg, S. Krug, R. Moumdjian, et al. 2008. Activated leukocyte cell adhesion molecule promotes leukocyte trafficking into the central nervous system. *Nat. Immunol.* 9:137–145. http://dx.doi.org/10.1038/ni1551

Cinamon, G., M. Matloubian, M.J. Lesneski, Y. Xu, C. Low, T. Lu, R.L. Proia, and J.G. Cyster. 2004. Sphingosine 1-phosphate receptor 1 promotes B cell localization in the splenic marginal zone. *Nat. Immunol.* 5:713–720. http://dx.doi.org/10.1038/ni1083

Cinamon, G., M.A. Zachariah, O.M. Lam, F.W. Foss Jr., and J.G. Cyster. 2008. Follicular shuttling of marginal zone B cells facilitates antigen transport. *Nat. Immunol.* 9:54–62. http://dx.doi.org/10.1038/ni1542

Crowther-Swanepoel, D., P. Broderick, Y. Ma, L. Robertson, A.M. Pittman, A. Price, P. Twiss, J. Vijayakrishnan, M. Qureshi, M.J. Dyer, et al. 2010. Fine-scale mapping of the 6p25.3 chronic lymphocytic leukaemia susceptibility locus. *Hum. Mol. Genet.* 19:1840–1845. http://dx.doi.org/10.1093/hmg/ddq044

Cyster, J.G., and S.R. Schwab. 2012. Sphingosine-1-phosphate and lymphocyte egress from lymphoid organs. *Annu. Rev. Immunol.* 30:69–94. http://dx.doi.org/10.1146/annurev-immunol-020711-075011

De Silva, N.S., G. Simonetti, N. Heise, and U. Klein. 2012. The diverse roles of IRF4 in late germinal center B-cell differentiation. *Immunol. Rev.* 247:73–92. http://dx.doi.org/10.1111/j.1600-065X.2012.01113.x

Di Bernardo, M.C., D. Crowther-Swanepoel, P. Broderick, E. Webb, G. Sellick, R. Wild, K. Sullivan, J. Vijayakrishnan, Y. Wang, A.M. Pittman, et al. 2008. A genome-wide association study identifies six susceptibility loci for chronic lymphocytic leukemia. *Nat. Genet.* 40:1204–1210. http://dx.doi.org/10.1038/ng.219

Dominguez-Sola, D., C.Y. Ying, C. Grandori, L. Ruggiero, B. Chen, M. Li, D.A. Galloway, W. Gu, J. Gautier, and R. Dalla-Favera. 2007. Non-transcriptional control of DNA replication by c-Myc. *Nature*. 448:445–451. http://dx.doi.org/10.1038/nature05953

Fabbri, G., S. Rasi, D. Rossi, V. Trifonov, H. Khiabanian, J. Ma, A. Grunn, M. Fangazio, D. Capello, S. Monti, et al. 2011. Analysis of the chronic lymphocytic leukemia coding genome: role of NOTCH1 mutational activation. *J. Exp. Med.* 208:1389–1401. http://dx.doi.org/10.1084/jem.20110921

Falini, B., M. Fizzotti, A. Pucciarini, B. Bigerna, T. Marafioti, M. Gambacorta, R. Pacini, C. Alunni, L. Natali-Tanci, B. Ugolini, et al. 2000. A monoclonal antibody (MUM1p) detects expression of the MUM1/IRF4 protein in a subset of germinal center B cells, plasma cells, and activated T cells. *Blood*. 95:2084–2092.

Ghia, P., N. Chiorazzi, and K. Stamatopoulos. 2008. Microenvironmental influences in chronic lymphocytic leukaemia: the role of antigen stimulation. *J. Intern. Med.* 264:549–562. http://dx.doi.org/10.1111/j.1365-2796.2008.02030.x

Guy, C.S., K.M. Vignali, J. Temirov, M.L. Bettini, A.E. Overacre, M. Smeltzer, H. Zhang, J.B. Huppa, Y.H. Tsai, C. Lobry, et al. 2013. Distinct TCR signaling pathways drive proliferation and cytokine production in T cells. *Nat. Immunol.* 14:262–270. http://dx.doi.org/10.1038/ni.2538

Hampel, F., S. Ehrenberg, C. Hojer, A. Draeseke, G. Marschall-Schröter, R. Kühn, B. Mack, O. Gires, C.J. Vahl, M. Schmidt-Supprian, et al. 2011. CD19-independent instruction of murine marginal zone B-cell development by constitutive Notch2 signaling. *Blood*. 118:6321–6331. http://dx.doi.org/10.1182/blood-2010-12-325944

Hoellenriegel, J., S.A. Meadows, M. Sivina, W.G. Wierda, H. Kantarjian, M.J. Keating, N. Giese, S. O'Brien, A. Yu, L.L. Miller, et al. 2011. The phosphoinositide 3′-kinase delta inhibitor, CAL-101, inhibits B-cell receptor signaling and chemokine networks in chronic lymphocytic leukemia. *Blood*. 118:3603–3612. http://dx.doi.org/10.1182/blood-2011-05-352492

Holl, E.K., B.P. O'Connor, T.M. Holl, K.E. Roney, A.G. Zimmermann, S. Jha, G. Kelsoe, and J.P. Ting. 2011. Plexin-D1 is a novel regulator of germinal centers and humoral immune responses. *J. Immunol.* 186:5603–5611. http://dx.doi.org/10.4049/jimmunol.1003464

Hozumi, K., N. Negishi, D. Suzuki, N. Abe, Y. Sotomaru, N. Tamaoki, C. Mailhos, D. Ish-Horowicz, S. Habu, and M.J. Owen. 2004. Delta-like 1 is necessary for the generation of marginal zone B cells but not T cells in vivo. *Nat. Immunol.* 5:638–644. http://dx.doi.org/10.1038/ni1075

Khalil, A.M., J.C. Cambier, and M.J. Shlomchik. 2012. B cell receptor signal transduction in the GC is short-circuited by high phosphatase activity. *Science*. 336:1178–1181. http://dx.doi.org/10.1126/science.1213368

Kiel, M.J., T. Velusamy, B.L. Betz, L. Zhao, H.G. Weigelin, M.Y. Chiang, D.R. Huebner-Chan, N.G. Bailey, D.T. Yang, G. Bhagat, et al. 2012. Whole-genome sequencing identifies recurrent somatic NOTCH2 mutations in splenic marginal zone lymphoma. *J. Exp. Med.* 209:1553–1565. http://dx.doi.org/10.1084/jem.20120910

Kin, N.W., D.M. Crawford, J. Liu, T.W. Behrens, and J.F. Kearney. 2008. DNA microarray gene expression profile of marginal zone versus follicular B cells and idiotype positive marginal zone B cells before and after immunization with Streptococcus pneumoniae. *J. Immunol.* 180:6663–6674.

Klein, U., Y. Tu, G.A. Stolovitzky, M. Mattioli, G. Cattoretti, H. Husson, A. Freedman, G. Inghirami, L. Cro, L. Baldini, et al. 2001. Gene expression profiling of B cell chronic lymphocytic leukemia reveals a homogeneous phenotype related to memory B cells. *J. Exp. Med.* 194:1625–1638. http://dx.doi.org/10.1084/jem.194.11.1625

Klein, U., S. Casola, G. Cattoretti, Q. Shen, M. Lia, T. Mo, T. Ludwig, K. Rajewsky, and R. Dalla-Favera. 2006. Transcription factor IRF4 controls plasma cell differentiation and class-switch recombination. *Nat. Immunol.* 7:773–782. http://dx.doi.org/10.1038/ni1357

Lu, R., K.L. Medina, D.W. Lancki, and H. Singh. 2003. IRF-4,8 orchestrate the pre-B-to-B transition in lymphocyte development. *Genes Dev.* 17:1703–1708. http://dx.doi.org/10.1101/gad.1104803

Lu, T.T., and J.G. Cyster. 2002. Integrin-mediated long-term B cell retention in the splenic marginal zone. *Science*. 297:409–412. http://dx.doi.org/10.1126/science.1071632

Martin, F., and J.F. Kearney. 2000. B-cell subsets and the mature preimmune repertoire. Marginal zone and B1 B cells as part of a "natural immune memory". *Immunol. Rev.* 175:70–79. http://dx.doi.org/10.1111/j.1600-065X.2000.imr017515.x

Mittrücker, H.W., T. Matsuyama, A. Grossman, T.M. Kündig, J. Potter, A. Shahinian, A. Wakeham, B. Patterson, P.S. Ohashi, and T.W. Mak. 1997. Requirement for the transcription factor LSIRF/IRF4 for mature B and T lymphocyte function. *Science*. 275:540–543. http://dx.doi.org/10.1126/science.275.5299.540

Moriyama, Y., C. Sekine, A. Koyanagi, N. Koyama, H. Ogata, S. Chiba, S. Hirose, K. Okumura, and H. Yagita. 2008. Delta-like 1 is essential for the maintenance of marginal zone B cells in normal mice but not in autoimmune mice. *Int. Immunol.* 20:763–773. http://dx.doi.org/10.1093/intimm/dxn034

Muppidi, J.R., T.I. Arnon, Y. Bronevetsky, N. Veerapen, M. Tanaka, G.S. Besra, and J.G. Cyster. 2011. Cannabinoid receptor 2 positions and retains marginal zone B cells within the splenic marginal zone. *J. Exp. Med.* 208:1941–1948. http://dx.doi.org/10.1084/jem.20111083

Nakamura, M., H. Yagi, S. Kayaba, T. Ishii, T. Gotoh, S. Ohtsu, and T. Itoh. 1996. Death of germinal center B cells without DNA fragmentation. *Eur. J. Immunol.* 26:1211–1216. http://dx.doi.org/10.1002/eji.1830260604

Nakamura, M., H. Yagi, T. Ishii, S. Kayaba, H. Soga, T. Gotoh, S. Ohtsu, M. Ogata, and T. Itoh. 1997. DNA fragmentation is not the primary event in glucocorticoid-induced thymocyte death in vivo. *Eur. J. Immunol.* 27:999–1004. http://dx.doi.org/10.1002/eji.1830270429

Nie, L., M. Xu, A. Vladimirova, and X.H. Sun. 2003. Notch-induced E2A ubiquitination and degradation are controlled by MAP kinase activities. *EMBO J.* 22:5780–5792. http://dx.doi.org/10.1093/emboj/cdg567

Ochiai, K., M. Maienschein-Cline, G. Simonetti, J. Chen, R. Rosenthal, R. Brink, A.S. Chong, U. Klein, A.R. Dinner, H. Singh, and R. Sciammas. 2013. Transcriptional regulation of germinal center B and plasma cell fates by dynamical control of IRF4. *Immunity*. 38:918–929. http://dx.doi.org/10.1016/j.immuni.2013.04.009

Pillai, S., and A. Cariappa. 2009. The follicular versus marginal zone B lymphocyte cell fate decision. *Nat. Rev. Immunol.* 9:767–777. http://dx.doi.org/10.1038/nri2656

Pillai, S., A. Cariappa, and S.T. Moran. 2005. Marginal zone B cells. *Annu. Rev. Immunol.* 23:161–196. http://dx.doi.org/10.1146/annurev.immunol.23.021704.115728

Ponader, S., S.S. Chen, J.J. Buggy, K. Balakrishnan, V. Gandhi, W.G. Wierda, M.J. Keating, S. O'Brien, N. Chiorazzi, and J.A. Burger. 2012. The Bruton tyrosine kinase inhibitor PCI-32765 thwarts chronic lymphocytic leukemia cell survival and tissue homing in vitro and in vivo. *Blood*. 119:1182–1189. http://dx.doi.org/10.1182/blood-2011-10-386417

Puente, X.S., M. Pinyol, V. Quesada, L. Conde, G.R. Ordóñez, N. Villamor, G. Escaramis, P. Jares, S. Beà, M. González-Díaz, et al. 2011. Whole-genome sequencing identifies recurrent mutations in chronic lymphocytic leukaemia. *Nature*. 475:101–105. http://dx.doi.org/10.1038/nature10113

Rosati, E., R. Sabatini, G. Rampino, A. Tabilio, M. Di Ianni, K. Fettucciari, A. Bartoli, S. Coaccioli, I. Screpanti, and P. Marconi. 2009. Constitutively activated Notch signaling is involved in survival and apoptosis resistance of B-CLL cells. *Blood*. 113:856–865. http://dx.doi.org/10.1182/blood-2008-02-139725

Rosati, E., R. Sabatini, F. De Falco, B. Del Papa, F. Falzetti, M. Di Ianni, L. Cavalli, K. Fettucciari, A. Bartoli, I. Screpanti, and P. Marconi. 2013. γ-Secretase inhibitor I induces apoptosis in chronic lymphocytic leukemia cells by proteasome inhibition, endoplasmic reticulum stress increase and notch down-regulation. *Int. J. Cancer*. 132:1940–1953. http://dx.doi.org/10.1002/ijc.27863

Rossi, D., V. Trifonov, M. Fangazio, A. Bruscaggin, S. Rasi, V. Spina, S. Monti, T. Vaisitti, F. Arruga, R. Famà, et al. 2012. The coding genome of splenic marginal zone lymphoma: activation of NOTCH2 and other pathways regulating marginal zone development. *J. Exp. Med.* 209:1537–1551. http://dx.doi.org/10.1084/jem.20120904

Saito, M., J. Gao, K. Basso, Y. Kitagawa, P.M. Smith, G. Bhagat, A. Pernis, L. Pasqualucci, and R. Dalla-Favera. 2007. A signaling pathway mediating downregulation of BCL6 in germinal center B cells is blocked by BCL6 gene alterations in B cell lymphoma. *Cancer Cell*. 12:280–292. http://dx.doi.org/10.1016/j.ccr.2007.08.011

Saito, T., S. Chiba, M. Ichikawa, A. Kunisato, T. Asai, K. Shimizu, T. Yamaguchi, G. Yamamoto, S. Seo, K. Kumano, et al. 2003. Notch2 is preferentially expressed in mature B cells and indispensable for marginal zone B lineage development. *Immunity*. 18:675–685. http://dx.doi.org/10.1016/S1074-7613(03)00111-0

Sciammas, R., A.L. Shaffer, J.H. Schatz, H. Zhao, L.M. Staudt, and H. Singh. 2006. Graded expression of interferon regulatory factor-4 coordinates isotype switching with plasma cell differentiation. *Immunity*. 25:225–236. http://dx.doi.org/10.1016/j.immuni.2006.07.009

Sciammas, R., Y. Li, A. Warmflash, Y. Song, A.R. Dinner, and H. Singh. 2011. An incoherent regulatory network architecture that orchestrates B cell diversification in response to antigen signaling. *Mol. Syst. Biol.* 7:495. http://dx.doi.org/10.1038/msb.2011.25

Shaffer, A.L., N.C. Emre, P.B. Romesser, and L.M. Staudt. 2009. IRF4: Immunity. Malignancy! Therapy? *Clin. Cancer Res.* 15:2954–2961. http://dx.doi.org/10.1158/1078-0432.CCR-08-1845

Shaffer, A.L. III, R.M. Young, and L.M. Staudt. 2012. Pathogenesis of human B cell lymphomas. *Annu. Rev. Immunol.* 30:565–610. http://dx.doi.org/10.1146/annurev-immunol-020711-075027

Shi, G.X., K. Harrison, G.L. Wilson, C. Moratz, and J.H. Kehrl. 2002. RGS13 regulates germinal center B lymphocytes responsiveness to CXC chemokine ligand (CXCL)12 and CXCL13. *J. Immunol.* 169:2507–2515.

Shukla, V., S. Ma, R.R. Hardy, S.S. Joshi, and R. Lu. 2013. A role for IRF4 in the development of CLL. *Blood*. 122:2848–2855. http://dx.doi.org/10.1182/blood-2013-03-492769

Stevenson, F.K., and F. Caligaris-Cappio. 2004. Chronic lymphocytic leukemia: revelations from the B-cell receptor. *Blood*. 103:4389–4395. http://dx.doi.org/10.1182/blood-2003-12-4312

Tan, J.B., K. Xu, K. Cretegny, I. Visan, J.S. Yuan, S.E. Egan, and C.J. Guidos. 2009. Lunatic and manic fringe cooperatively enhance marginal zone B cell precursor competition for delta-like 1 in splenic endothelial niches. *Immunity*. 30:254–263. http://dx.doi.org/10.1016/j.immuni.2008.12.016

Tanigaki, K., H. Han, N. Yamamoto, K. Tashiro, M. Ikegawa, K. Kuroda, A. Suzuki, T. Nakano, and T. Honjo. 2002. Notch-RBP-J signaling is involved in cell fate determination of marginal zone B cells. *Nat. Immunol.* 3:443–450. http://dx.doi.org/10.1038/ni793

Thomas, M., M. Calamito, B. Srivastava, I. Maillard, W.S. Pear, and D. Allman. 2007. Notch activity synergizes with B-cell-receptor and CD40 signaling to enhance B-cell activation. *Blood*. 109:3342–3350. http://dx.doi.org/10.1182/blood-2006-09-046698

Tran, I.T., A.R. Sandy, A.J. Carulli, C. Ebens, J. Chung, G.T. Shan, V. Radojcic, A. Friedman, T. Gridley, A. Shelton, et al. 2013. Blockade of individual Notch ligands and receptors controls graft-versus-host disease. *J. Clin. Invest.* 123:1590–1604. http://dx.doi.org/10.1172/JCI65477

Tsuboi, K., S. Iida, H. Inagaki, M. Kato, Y. Hayami, I. Hanamura, K. Miura, S. Harada, M. Kikuchi, H. Komatsu, et al. 2000. MUM1/IRF4 expression as a frequent event in mature lymphoid malignancies. *Leukemia*. 14:449–456. http://dx.doi.org/10.1038/sj.leu.2401696

Wang, H., N. Beaty, S. Chen, C.F. Qi, M. Masiuk, D.M. Shin, and H.C. Morse III. 2012. The CXCR7 chemokine receptor promotes B-cell retention in the splenic marginal zone and serves as a sink for CXCL12. *Blood*. 119:465–468. http://dx.doi.org/10.1182/blood-2011-03-343608

Welcker, M., and B.E. Clurman. 2008. FBW7 ubiquitin ligase: a tumour suppressor at the crossroads of cell division, growth and differentiation. *Nat. Rev. Cancer*. 8:83–93. http://dx.doi.org/10.1038/nrc2290

Wu, Y., C. Cain-Hom, L. Choy, T.J. Hagenbeek, G.P. de Leon, Y. Chen, D. Finkle, R. Venook, X. Wu, J. Ridgway, et al. 2010. Therapeutic antibody targeting of individual Notch receptors. *Nature*. 464:1052–1057. http://dx.doi.org/10.1038/nature08878

Ye, B.H., G. Cattoretti, Q. Shen, J. Zhang, N. Hawe, R. de Waard, C. Leung, M. Nouri-Shirazi, A. Orazi, R.S. Chaganti, et al. 1997. The BCL-6 proto-oncogene controls germinal-centre formation and Th2-type inflammation. *Nat. Genet.* 16:161–170. http://dx.doi.org/10.1038/ng0697-161